INL/EXT-08-14053

PINS Measurements of Explosive Simulants for Cargo Screening

E. H. Seabury

June 2008

The INL is a U.S. Department of Energy National Laboratory
operated by Battelle Energy Alliance

INL/EXT-08-14053

PINS Measurements of Explosive Simulants for Cargo Screening

E. H. Seabury

June 2008

Idaho National Laboratory
Idaho Falls, Idaho 83415

http://www.inl.gov

Prepared for the
Battelle Memorial Institute
and for the
U.S. Department of Energy
Under DOE Idaho Operations Office
Contract DE-AC07-05ID14517

CONTENTS

FIGURES

PINS Measurements of Explosive Simulants for Cargo Screening

1. INTRODUCTION

As part of its efforts to prevent the introduction of explosive threats on commercial flights, the Transportation Security Administration (TSL) is evaluating new explosives detection systems (EDSs) for use in air cargo inspection. The TSL has contracted Battelle to develop a new type of explosives simulant to assist in this development. These are designed to mimic the elemental profile (C, H, N, O, etc.) of explosives as well as their densities. Several "neutron in—gamma out" (n,ɣ) techniques have been considered to quantify the elemental profile in these new simulants and the respective explosives. The method chosen by Battelle is Portable Isotopic Neutron Spectroscopy (PINS) [1], developed by Idaho National Laboratory (INL). Battelle wishes to validate that the simulants behave like the explosive threats with this technology.

Presently, most interrogation of aircraft luggage for bulk explosives is performed with X-ray and computed tomography (CT) systems. However, cargo inspection requires the greater penetrating power neutrons or high-energy gamma rays. A variety of high energy photon and (n, ɣ) techniques have been utilized to detect explosives in different settings, aircraft cargo being perhaps the most challenging. Existing X-ray and CT explosives simulants do not match the overall chemical profile (percent C, H, N, O, etc.) of explosives. They often contain extraneous materials (e.g. Fe_2O_3, SiO_2, and B_4C) in order to adjust CT number, Effective Average Atomic Number (Z_{eff}), and density. Many of these added elements (Fe, Si, and B) are not found in explosives. Hence these older explosives simulants are not suitable for neutron or gamma-ray techniques. Their presence may introduce artifacts into the spectrum obtained and could potentially interfere with proper interrogation. Hence there is a need for new simulants to assist the development of neutron- and gamma-based technologies for explosives interrogation. To address this situation Battelle has developed a series of explosives simulants. Battelle initially contracted Van Aken Technologies to develop such a line of explosives simulants. Battelle later developed their own line of explosives simulants using different materials.

1.1 Neutron sources and neutron-induced reactions

Gammas rays are produced primarily through two neutron interactions on atomic nuclei. One of these reactions is thermal neutron capture. In this reaction, a low-energy, slow neutron is captured by an atomic nucleus which then immediately emits one or more gamma rays. A second reaction occurs when a more energetic neutron inelastically scatters off of an atomic nucleus, which is left in an excited state. The nucleus then de-excites by gamma-ray emission. The choice of a neutron source in an interrogation system depends on whether thermal capture, inelastic scattering, or both are necessary to observe all of the elements of interest.

Explosives consist primarily of the elements carbon, oxygen, nitrogen, and hydrogen. The elemental capture cross sections for carbon and oxygen are 0.0035 barns and 0.00019 barns respectively. The elemental capture cross sections for hydrogen and nitrogen are 0.33 and 0.0795 barns respectively. Carbon and oxygen seldom react with thermal neutrons and are more likely to react with higher energy neutrons through neutron inelastic scattering. This requires neutrons of energy at least 4.4 MeV in the case of the carbon and 6.13 MeV in the case of oxygen. Hydrogen nuclei cannot be excited by inelastic scattering and can only be detected through thermal neutron capture. The identification of explosives requires both thermal neutrons and neutrons exceeding 6.13 MeV in energy.

The energy distributions of three common neutron sources are shown in Figure 1. The PINS system usually uses a Californium-252 source to interrogate suspected chemical warfare materiel (CWM). CWM consists of a variety of elements of interest and the large energy distribution of neutrons from ^{252}Cf spontaneous fission allows excitation of many of these atomic nuclei. Carbon and oxygen are not generally observed in the spectra from ^{252}Cf based interrogation however. This is due to the relatively low number of higher-energy neutrons produced in ^{252}Cf fission. Similarly, the 2.5 MeV neutrons produced in a deuterium-deuterium (DD) neutron generator are too low in energy to excite carbon and oxygen.

In order to readily excite carbon and oxygen nuclei, a deuterium-tritium (DT) neutron generator is used. The DT neutron generator consists of a small particle accelerator with target. The particle beam consists of deuterium and tritium ions, which then impinge on a target previously impregnated with deuterium and tritium. Some of these nuclei undergo the fusion reaction below

$$D + T \rightarrow {}^{4}He + n$$

resulting in the production of an alpha particle and a neutron of about 14 MeV in energy. These neutrons readily excite carbon and oxygen nuclei through inelastic scattering. Thermal neutrons are available from some of these higher-energy neutrons slowing down or moderating in surrounding materials and in the test item itself.

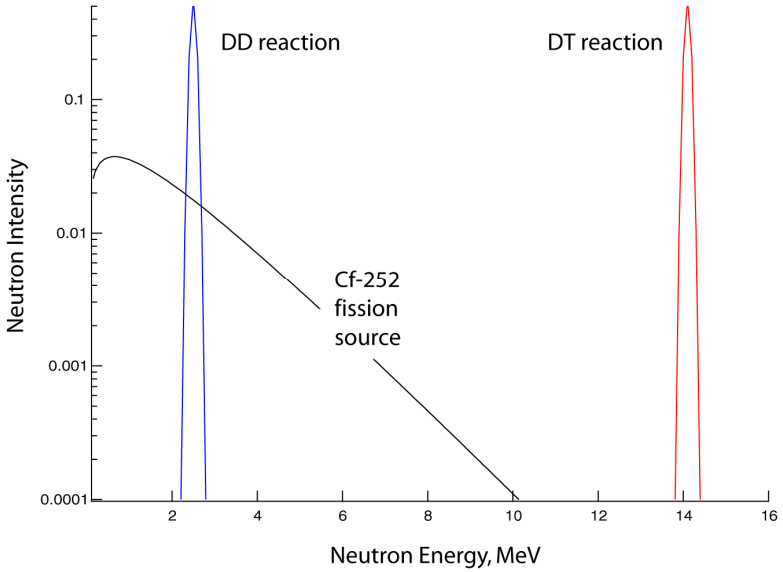

Figure 1. Californium-252, deuterium-deuterium (DD) fusion, and deuterium-tritium (DT) fusion neutron spectra.

2. EXPERIMENTAL PROCEDURES

The experimental arrangement for measuring both the explosive simulants and their respective explosives was simple, consisting of only one detector, a neutron source, and appropriate shielding. Because the simulants were of relatively small masses for neutron interrogation, they were assessed with both a neutron generator-based and a ^{252}Cf -based system. This was in order to provide adequate hydrogen and nitrogen excitation without relying heavily on moderation of neutrons within the test samples themselves.

2.1 Californium neutron source-based system

The Cf-based PINS system was operated with a 9.4 μg ^{252}Cf neutron source, producing approximately 20 million neutrons per second. Gamma rays were detected with a high-purity germanium (HPGe) detector of approximately 45% relative efficiency. The HPGe detector was shielded from direct view of the neutron source by two 4 x 4 x 2 inch blocks of tungsten, and a bismuth collimator shielded the detector from background gamma rays produced by neutron interactions in the floor. The ^{252}Cf source experimental setup is depicted schematically in Figure 2.

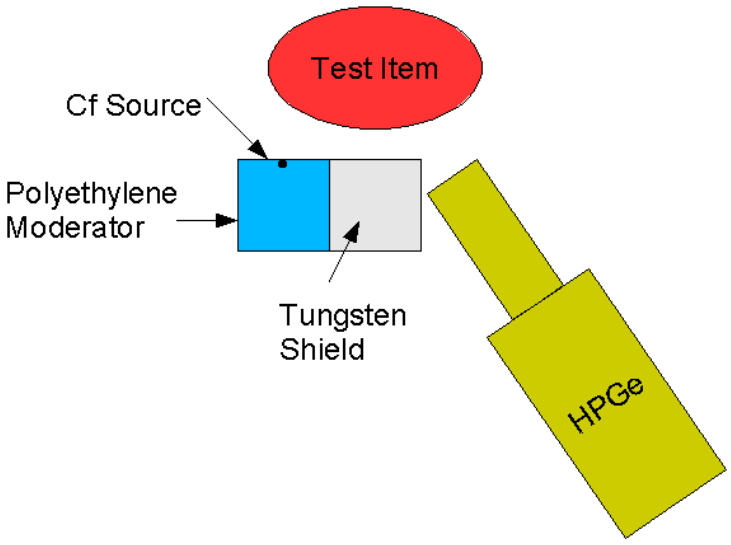

Figure 2. PINS ^{252}Cf source experimental setup.

2.2 DT neutron generator-based system.

A DT neutron generator was used as the neutron source for these experiments. The neutron generator can produce approximately 1E+08 n/s, but was operated at an output of approximately 3E+07 n/s In order to reduce the dead time on the data acquisition electronics for the HPGe. The experimental arrangement can be seen in Figure 3 below. The neutron generator was placed in a polyethylene moderator block and the detector was shielded from direct view of the generator and polyethylene by lead bricks. The detector was also shielded from below and above by lead bricks to minimize detection of gamma rays from materials surrounding the experimental setup.

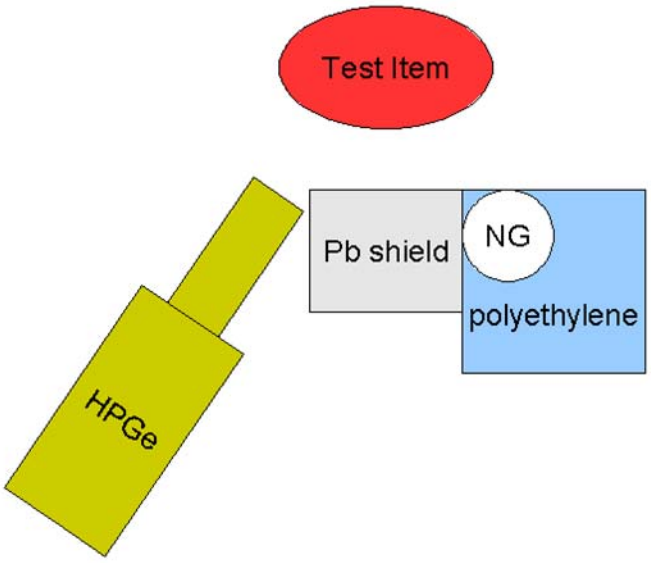

Figure 3. PINS DT source experimental setup**.**

2.3 Operating procedures

For both setups a background spectrum was measured at the beginning of each day. These spectra were used to subtract the portion of the gamma spectrum for a test item that was due to the surrounding materials. Test items were placed in front of the systems and spectra were measured, with intermediate spectra being saved every 1000 live seconds. Replicate measurements of a particular test item were made by stopping the data acquisition, removing or turning off the neutron source, and finally removing and then either replacing the test item or substituting a new one. This resulted in slight geometry changes between replicate measurements.

The explosive simulants for C-4, Semtex 1-A, Detasheet, Black Powder. Z-powder, Blastrite-3, Red Dot, and TNT were all measured with both the ^{252}Cf based system as well as with the neutron generator system. These measurements occurred at the PINS laboratory in Idaho Falls, ID. The measurements of actual explosives were performed only with the DT generator-based system at the PBF facility of Idaho National Laboratory. ^{252}Cf is presently unavailable at the PBF facility where live explosives can be used.

The simulants were all of relatively small mass, on the order of 1 kg of test material, whereas much larger masses of explosives were used. The explosives masses were on the order of 5 kg or more in order to obtain better statistics and more thermal neutron flux within the explosive iteself. The only exception to this was the Semtex-1A. There was only approximately 1 kg of this explosive available at INL for testing, comprised of a collection of smaller masses on the order of 50-200 grams.

3. DATA ANALYSIS

The data for these measurements consisted of gamma-ray spectra for each of the simulants and each of their respective explosives. The spectra were examined for peaks of specific energies, characteristic of particular elements. For example, Figure 4 below shows a segment of the gamma-ray spectrum for C-4. In the spectrum, the 2223 keV peak from thermal neutron capture on hydrogen can be clearly seen. Other peaks of interest are the 6129 keV peak from inelastic scattering off ^{16}O, the 10.8 Mev peak from thermal neutron capture on ^{14}N, and the 4439 keV peak from inelastic scattering off ^{12}C. The 4439 keV peak is shown in Figure 5. This peak is much broader than others of similar energy due to Doppler broadening of the gamma ray. A final peak of interest in these measurements was the 2230 keV peak from inelastic scattering off ^{32}S and the 2813 keV peak from inelastic scattering off ^{39}K.

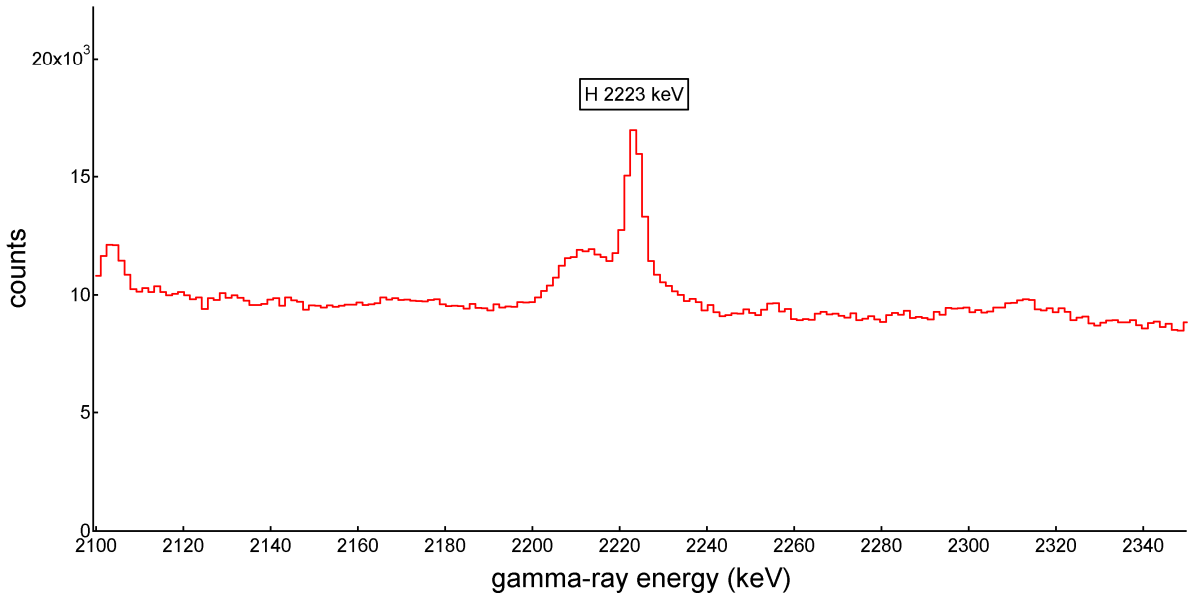

Figure 4. Hydrogen region in spectrum from C-4.

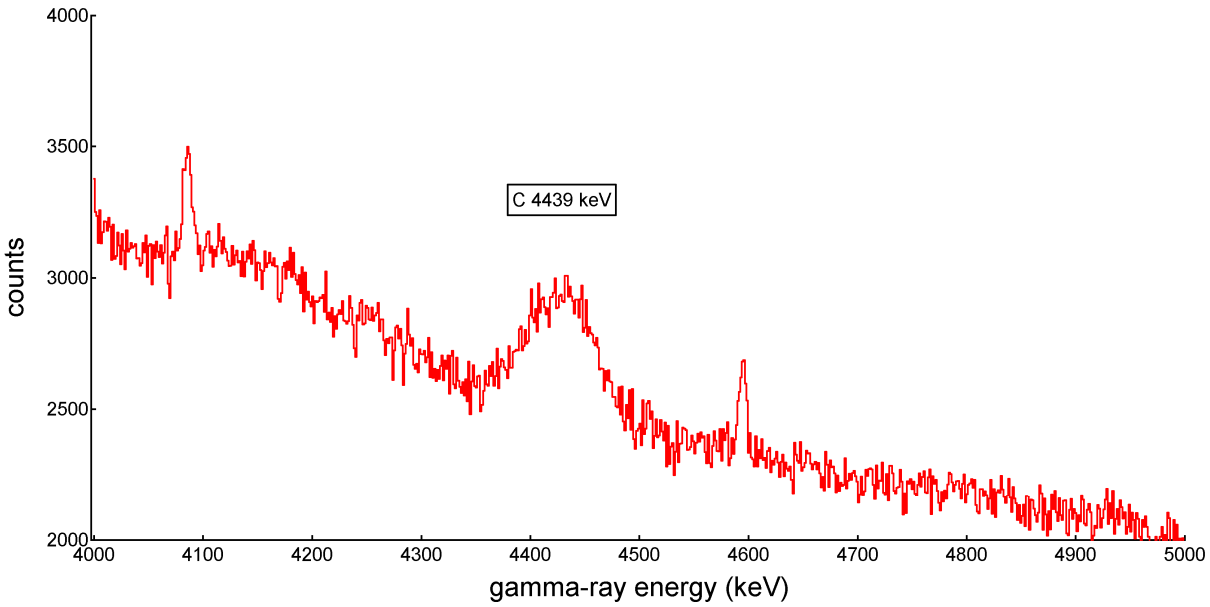

Figure 5. Carbon region in spectrum from C-4**.**

In addition to examining the spectra for the expected peaks from the elements comprising explosives, the spectra from the simulants were examined for additional peaks from elements not expected to be in explosives, such as B, Fe, and Si.

3.1 Background Subtraction

In order to determine the areas of peaks of interest, the background spectra had first to be subtracted from those of the test items. These background spectra were of a shorter measurement time than those of either the simulants or explosives. The neutron generator output does vary somewhat over time and the appropriate multiple of the background spectrum to subtract cannot be accurately determined by the ratio of measurement times. Instead the area of a peak in the spectrum that is not expected to be due to the test item is used to determine the correct ratio of background to foreground spectra. In these measurements, the 2614 keV peak from inelastic scattering off lead was used. This gamma ray is expected to be due entirely to the shielding material surrounding the detector, and therefore a good measure of the total neutron generator output during the counting time. Figure 6 shows the hydrogen region of the same spectrum shown in Figure 4 after background subtraction. As can be seen in the figure, the large multiplet of peaks to the left of the hydrogen peak is largely removed after subtraction. This multiplet is due to neutron interactions on the detector itself. Similarly, gamma rays from interactions on the floor or shielding material are also largely removed in the subtraction.

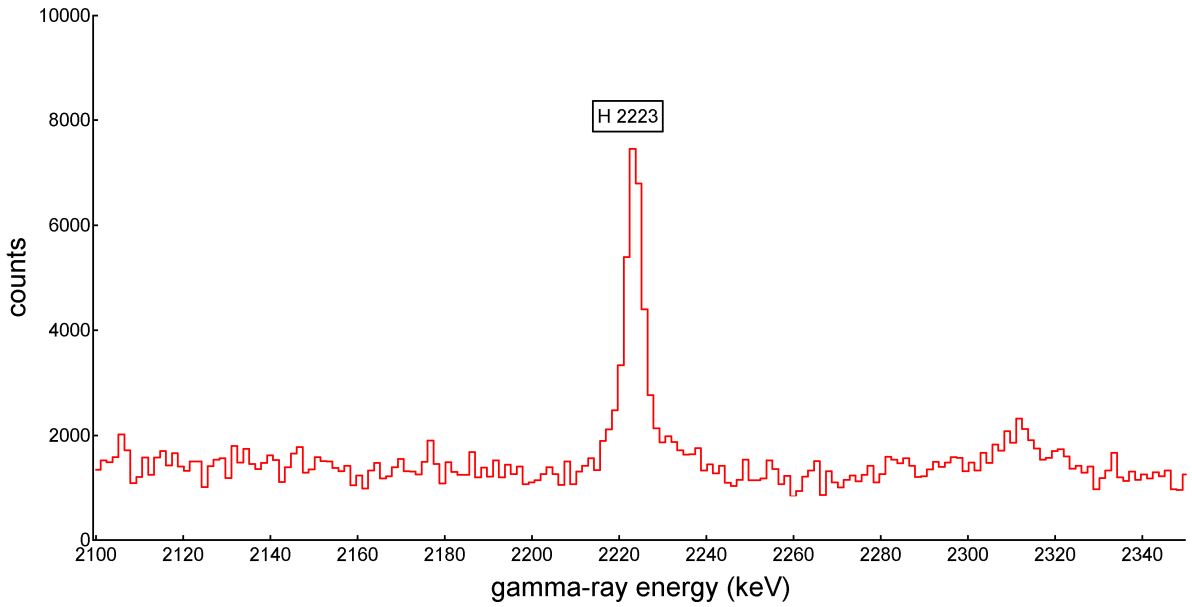

Figure 6. Hydrogen region in spectrum from C-4 after background subtraction**.**

3.2 Peak Areas and Elemental Ratios

Peak areas are determined, after background subtraction, by fitting a peak or set of peaks with gaussian curves over a flat background. The Gauss program, developed at INL [2], was used to fit peaks. A sample screenshot from the program is shown in Figure 7, where the same peak from thermal neutron capture on hydrogen is fit with a set of gaussian curves. The peak areas, full widths at half maximum, and uncertainties are reported by the program. The peaks due to neutron interactions on carbon, oxygen, hydrogen, and sulfur were fit in this manner. Nitrogen peak areas were determined differently.

Nitrogen reacts very weakly with fast neutron and weakly with thermal neutrons. The gamma ray peak of interest from thermal neutron capture on nitrogen has an energy of 10.8 MeV. The HPGe detector is inefficient at detecting gamma rays of such high energy, and nitrogen peaks in the explosive and simulant spectra are rarely able to be fit with gaussians due to the poor statistics. Instead, a summing process is used. A nine-channel wide region of the spectrum where the nitrogen peak is expected to be from the energy calibration is summed, as well as separate sums of forty-channel wide regions both higher and lower in energy. The higher and lower energy regions provide the background counts to be subtracted from the nitrogen region. The normalized difference provides the net nitrogen counts. This procedure is also performed on the first escape peak of the nitrogen 10.8 MeV peak in order to obtain better statistics. From the peak areas, elemental ratios can be determined.

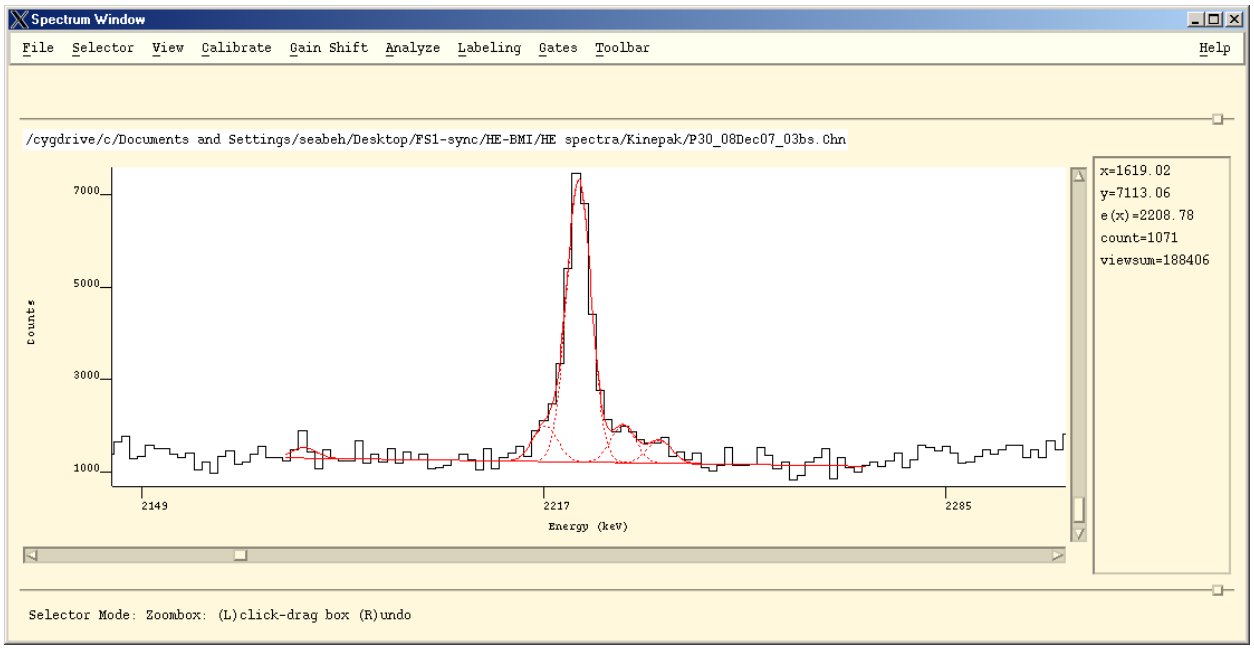

Figure 7. Gaussian fit of hydrogen peak**.**

The elemental ratios described here are ratios of gamma-ray peak areas, not ratios of elemental concentrations or masses within the test items. These ratios are useful in particular for characterizing the responses of materials to the high-energy neutrons produced by a DT generator. The strongest gamma rays that correspond to interactions with hydrogen and nitrogen are due to thermal capture on those elements. The energy distribution of neutrons within an item however is strongly dependent both on the absolute quantity of test material present, as well as its geometry. A sheet of material produces a significantly different neutron-induced gamma response than a sphere of the same material with the same mass. In order to reduce effects of geometry and size, ratios of gamma rays produced by neutron interactions of approximately the same neutron energy are taken. In our measurements we are mostly concerned with the ratios of hydrogen to nitrogen (thermal capture) and carbon to oxygen (inelastic scattering). The neutron-energy thresholds for inelastic scattering off carbon and oxygen are close enough in energy that geometry and mass effects are removed [3].

The peak areas for the 2223 keV hydrogen peak, the 10829 keV nitrogen peak, and its first escape peak at 10318 keV were obtained from the spectra for all of the explosives and simulants. These peak areas with their associated uncertainties can be found in Appendix A. The hydrogen to nitrogen ratio reported in the next section is the ratio of the hydrogen peak area to the sum of the nitrogen and nitrogen-escape peak areas. The carbon to oxygen ratio reported in the next section is the ratio of the 4439 keV carbon peak to the sum of the 6129 keV oxygen peak and its first excape peak at 5618 keV. The oxygen second escape peak at 5107 keV was not used as it is contaminated by a nitrogen inelastic scattering peak at 5104 keV. In addition to the above peaks, the 2230 keV peak from inelastic scattering off ^{32}S was also determined for the cases of the black powder and its simulant.

4. RESULTS

The peak area ratios were divided into two types: those from inalstic scattering and those from thermal neutron capture. The sections below describe the results for each type of ratio.

4.1 Inelastic scattering peak area ratios

The table below shows the carbon to oxygen ratios for the explosives and the simulants. As can be seen in the table, there is good agreement between the simulant and explosives for Detasheet, Semtex 1-A, and TNT. The C-4 and Red Dot ratios for the explosives and simulants are within two standard deviations of each other.

The explosive Detagel, was used as a substitute for Blastrite-3. The C/O ratio for the Detagel and the simulated Blastrite-3 are also within two standard deviations of each other. The black powder explosive and simulant have a large disagreement however. Part of this disagreement could be due to the packaging of the simulated black powder. This simulant was in three plastic bottles, although each bottle was less than half full. The plastic could be impacting the overall carbon to oxygen ratio. The explosive black powder was also in plastic bottles, but these bottles were approximately two-thirds full. The Z-Powder explosive and simulant also have strongly disagreeing carbon to oxygen ratios,.

Explosive	**HE C/O Ratio**	**Simulant C/O Ratio**
Black Powder	1.07 (0.12)	2.49 (0.06)
Blastrite-3		1.06 (0.27)
C-4	1.36 (0.15)	1.87 (0.28)
Detagel	0.43 (.07)	
Detasheet	1.32 (0.17)	1.27 (0.14)
Red Dot	1.32 (0.09)	2.03 (0.38)
Semtex 1-A	1.62 (0.01)	1.41 (0.28)
TNT	1.98 (0.16)	1.97 (0.51)
Z-Powder	0.58 (0.05)	1.07 (0.01)

Table 1. C/O ratios for explosives and simulants**.**

Table 2 shows the carbon to sulfur, sulfur to oxygen, and carbon to potassium ratios for the black powder explosive and simulant. As can be seen in the table, the carbon to sulfur ratio for the simulant is approximately a factor of two higher than that of the explosive. The sulfur to oxygen ratios however are in good agreement, and the carbon to potassium ratios are in relatively good agreement.. The discrepancy between the carbon to sulfur and carbon to oxygen ratios between the black powder simulant and explosive indicates that the carbon content of the simulant in its measurement configuration is likely higher than that of the real explosive. This is also indicated by the carbon to potassium ratio.

Explosive	**HE C/S Ratio**	**Simulant C/S Ratio**	**HE S/O Ratio**	**Simulant S/O Ratio**	**Explosive C/K Ratio**	**Simulant C/K Ratio**
Black Powder	2.11 (0.56)	4.77 (0.97)	0.53 (0.11)	0.51 (0.07)	3.46 (.26)	4.29 (.37)

Table 2. C/S, S/O, and C/K ratios for explosives and simulants**.**

4.2 Thermal neutron capture elemental ratios

As described in previous sections, the primarly elemental ratio for thermal neutron capture is that of hydrogen to nitrogen. These spectra for these ratios were measured with the 252Cf – based system for the simulants in order to obtain better counting statistics on the nitrogen peaks. The ratios for the explosives were determined from the same spectra from which inelastic scattering ratios were obtained.

Table 3 shows the hydrogen to nitrogen ratios for both the explosives and their simulants. Some of the explosives measurements resulted in negative peak areas for nitrogen after background subtraction. These values were ignored as being non-physical in determining the average value of the hydrogen to nitrogen ratio, but were included in determining the standard deviation of the average. As can be seen in the table, while there is general agreement between the explosives and their simulants in the hydrogen to nitrogen ratio, the large variance in the ratios among sets of replicate measurements do not allow us to determine whether the simulants accurately represent the true elemental ratios present in the explosives. Even the ^{252}Cf-based measurements on the simulants showed a high degree of variance among sets of replicate measurements. Nitrogen was detected in all of the ^{252}Cf-based measurements however.

Explosive	**HE H/N Ratio**	**Simulant ^{252}Cf H/N Ratio**
Black Powder	404 (4000)	967 (490)
Blastrite-3		1221 (239)

C-4	125 (492)	552 (212)
Detagel	258 (11)	
Detasheet	248 (1567)	815 (111)
Red Dot	331 (201)	1977 (972)
Semtex 1-A	133 (316)	676 (86)
TNT	624 (225)	742 (419)
Z-Powder	100 (25)	1526 (594)

Table 3. H/N ratios for explosives and simulants**.**

4.3 Spectral overlays

In addition to measuring peak areas and elemental ratios, another method for comparing the simulants with the explosives is to simply overlay spectra and visually examine the differences and similarities between the two. Examples of this can be seen in figures 8, 9 and 10. Figure 8 shows an overlay of the hydrogen region of the spectra for the Red Dot explosive and simulant,figure 9 shows the oxygen region and figure 10 the nitrogen region.

The hydrogen peaks for the explosive and simulant spectra are evident in figure 8. Direct comparisons of peak height inidicate the relative amounts of simulant and explosive more than the fraction of hydrogen in either the simulant or the explosive. The two peaks to the left of the hydrogen peak in the explosive spectrum are present in the background and in all the explosive spectra. Overlays of all the explosive and simulant spectra can be found in Appendix B. The simulants showed all the peaks of key elements that were present in the explosives spectra with the only exception being the Z-powder simulant. The Z-powder explosive showed strong chlorine peaks that were not evident in the simulant. These peaks were also not evident in the background spectra and can be attributed entirely to the explosive itself.

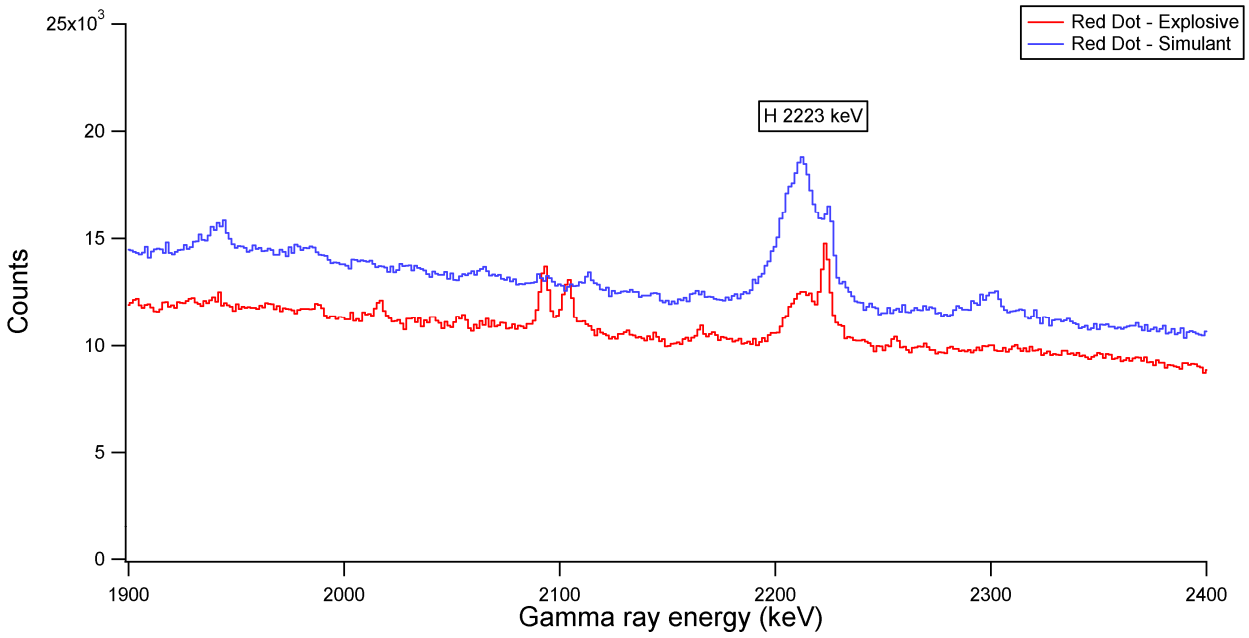

Figure 8. Hydrogen region in Red Dot explosive and simulant spectra.

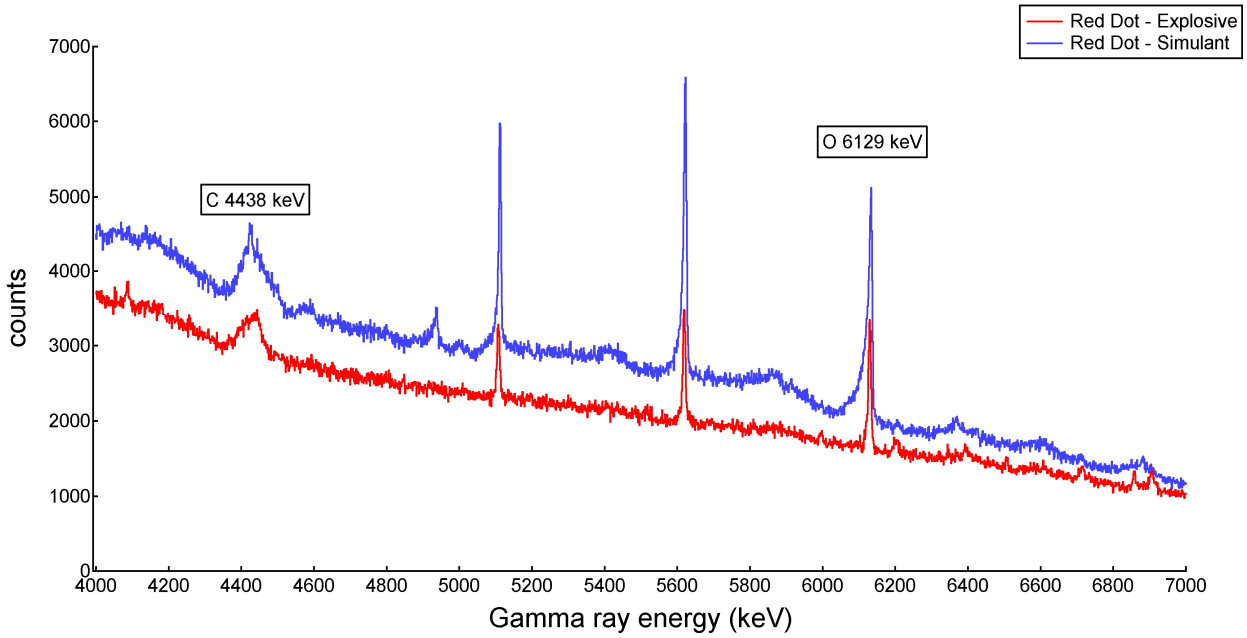

Figure 9. Oxygen region in Red Dot explosive and simulant spectra.

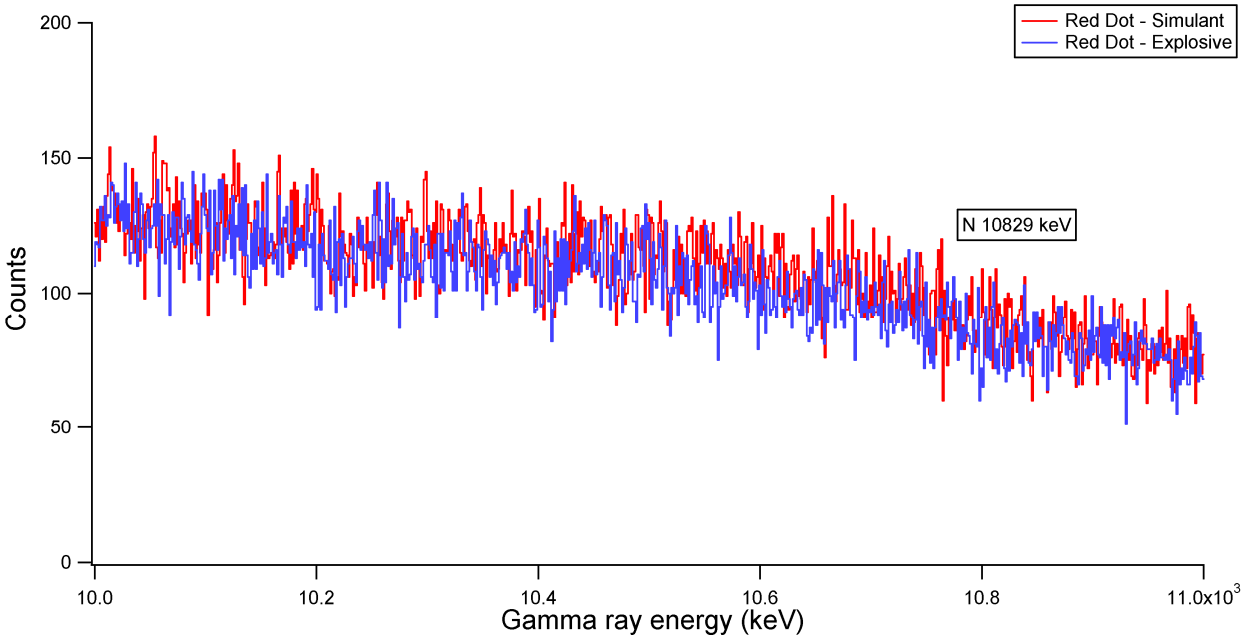

Figure 10. Nitrogen region in Red Dot explosive and simulant spectra.

5. CONCLUSIONS

As can be seen in the previous section, in general there is relative agreement between the explosive and simulant carbon to oxygen ratios. One major exception to this is for the black powder simulant, which had a significantly higher carbon to oxygen ratio. The carbon to sulfur and carbon to potassium ratios showed similar disagreement between the simulant and explosive, indicating that there might be significantly higher carbon in the black powder simulant as it was configured for measurement. This was also indicated by the agreement between the sulfur to oxygen ratios between the simulant and the explosive. The Z-powder simulant also had significant disagreement with the explosive in its carbon to oxygen ratio, in addition to showing no sign of the strong chlorine peaks present in the explosive.

The hydrogen to nitrogen ratios, although in general agreement between the simulants and the explosives, show a high degree of variance among replicate measurements. This is due to the poor statistics on the nitrogen thermal capture peaks.

6. REFERENCES

1. A.J. Caffrey, J.D. Cole, R.J. Gehrke, and R.C. Greenwood, "Chemical warfare agent and high explosive identification by spectroscopy of neutron-induced gamma rays", IEEE Transactions on Nuclear Science, **39** (1992) pp 1422-1426

2. A.E. Egger, M.H. Putnam, R.G. Helmer, A.J. Caffrey, and R.C. Greenwood, "Gauss IX: An Interactive Program for the Analysis of Gamma-Ray Spectra from Ge Semiconductor Detectors," *IEEE Transactions on Nuclear Science* **42** (1994) pp. 267-271.

3. E.H. Seabury and A.J. Caffrey, "Explosive Detection by PGNAA", Idaho National Engineering and Environmental Laboratory Report INEEL-EXT-04-02475, 2004.

Appendix A

Peak Areas for Explosives and Simulants

Appendix A
Peak Areas for Explosives and Simulants

Simulant Measurements ^{252}Cf source

Simulant	File-ID	Live Time	H-2223	unc	N-Sum	Unc	Nsum-Ne	Nsum-N	Nsum-sum	unc
Black Powder	P15_13Jul07_42	6000	26136	250	51.7	9.466784	36.575	6.7	43.275	7.924083
Black Powder	P15_12Jul07_36	6000	28204	265	34.8	8.823831	22.5625	15.35	37.9125	9.613032
Black Powder	P15_02Aug07_06	6000	22329	241	28.9	7.924645	3.825	16.5125	20.3375	5.576729
Black Powder	P15_06Aug07_15	6000	27315	257	15.8	7.262231	11.3875	4.05	15.4375	7.095613
Black Powder	P15_24Aug07_06	6000	14970	222	23.2	7.566373	20.925	3.2	24.125	7.868049
blastrite	P15_06Sep07_06	3000	119584	541	77.8	11.89664	63.8125	12.812	76.6245	11.71689
blastrite	P15_06Sep07_12	3000	102675	501	98.3	12.52996	90.7875	13.4875	104.275	13.29158
blastrite	P15_06Sep07_18	3000	105002	523	82	11.8072	61.7625	17.05	78.8125	11.34823
blastrite	P15_07Sep07_06	3000	130272	533	132	14.35584	104.5	24.525	129.025	14.03228
blastrite	P15_07Sep07_12	3000	90645	489	71.7	10.8706	60.35	13.9625	74.3125	11.26669
C-4	P15_12Jul07_06	3000	44213	331	131.5	12.75813	93.825	37.987	131.812	12.7884
C-4	P15_12Jul07_42	3000	34305	299	91.6	11.07881	69.275	30	99.275	12.00708
C-4	P15_02Aug07_15	3000	17924	206	32.9	9.124144	18.675	4.0875	22.7625	6.312715
C-4	P15_06Aug07_09	3000	25976	232	44.5	8.504117	10.8625	24.225	35.0875	6.705353
C-4	P15_23Aug07_03	3000	21939	226	42.1	8.184131	33.2125	6.6875	39.9	7.756457
Detasheet	P15_13Jul07_24	3000	44859	344	60.2	9.381365	43.45	20.112	63.562	9.905287
Detasheet	P15_12Jul07_18	3000	43932	323	54.7	9.042677	48.6875	12.6625	61.35	10.14201
Detasheet	P15_16Jul07_03	3000	58225	363	65.5	9.947864	56.1625	15.3	71.4625	10.85342
Detasheet	P15_16Jul07_06	3000	40260	312	43	8.19878	38.1625	10.4375	48.6	9.266529
Detasheet	P15_17Jul07_06	3000	40550	318	41	8.112336	38.35	11.89	50.24	9.94058
Detasheet	P15_17Jul07_12	3000	40979	316	41.6	8.19878	33.575	6.775	40.35	7.952423
RedDot	P15_13Jul07_12	6000	62169	461	70.7	10.84666	48.925	21.112	70.037	10.74494
RedDot	P15_02Aug07_12	6000	61839	3716	56.9475	10.30049	10.3625	8.6625	19.025	3.441182
RedDot	P15_06Aug07_21	6000	65653	3837	47.384	9.381365	22.8875	10.7125	33.6	6.652327
RedDot	P15_24Aug07_12	6000	65608	3387	38.7	8.91852	29.8625	6.2626	36.1251	8.325127
Semtex	P15_13Jul07_18	3000	44181	345	66.6	9.679876	48.775	24.225	73	10.61007
Semtex	P15_12Jul07_24	3000	45931	322	75.3	10.13558	50.2999	21.4625	71.7624	9.65941

Semtex	P15_16Jul07_10	4000	66639	389	109.7	12.14331	85.9	23.49	109.39	12.109
Semtex	P15_16Jul07_12	2000	29450	260	39.1	7.566373	32.737	8.025	40.762	7.887992
Semtex	P15_16Jul07_15	3000	45041	331	58.9	9.360021	35.85	20.112	55.962	8.893133
TNT	P15_13Jul07_30	3000	27562	290	67.3	9.689685	55.7875	17.8625	73.65	10.60394
TNT	P15_12Jul07_12	3000	32679	293	79	10.27278	65.45	19.2	84.65	11.00748
TNT	P15_06Aug07_06	6000	66024	4163	60.4	10.31746	46.075	11.55	57.625	9.843439
TNT	P15_24Aug07_15	3000	29344	2912	29.9	7.211103	30.2625	-2.65	27.6125	6.659417
Z-Powder	P15_06Sep07_03	3000	29678	2747	16	6.324555	8.125	6.4625	14.5875	5.766216
Z-Powder	P15_06Sep07_09	3000	28453	3257	18.3	6.441273	11.2375	1.5875	12.825	4.514171
Z-Powder	P15_06Sep07_15	3000	28453	3257	31.2	7.206941	30.475	3.35	33.825	7.813294
Z-Powder	P15_07Sep07_03	3000	32151	4013	24.1	6.935416	24.25	5.575	29.825	8.582937
Z-Powder	P15_07Sep07_09	3000	35016	3379	25.4	7.119691	19.125	4.8875	24.0125	6.730771

Simulant Measurements DT source

Simulant	File-ID	Live Time	Bi-1608	unc	S-2230	unc	K-2813	Unc	C-4439	unc		uncr	O-5618	unc	O-6129	unc
Blastrite-3	P15_04Sep07_07	6000	125210	2000					17636		260	1410.88	8223	141	8890	157
Blastrite-3	P15_04Sep07_13	6000	111222	2000					17702		2000	1416.16	8626	113	6246	99
Blastrite-3	P15_05Sep07_07	6000	109614	2000					17815		245	1425.2	13986	216	11118	184
Blastrite-3	P15_05Sep07_19	6000	134933	2000					16125		212	1290	6906	115	5364	118
Black Powder	P15_08Aug07_07	6000	144797	849	6872	119	8390	701	36859		272	2948.72	6129	96	6913	113
Black Powder	P15_08Aug07_22	3000	681170	587	4904	93	4230	619	15830		179	1266.4	5523	80	4099	68
Black Powder	P15_09Aug07_13	6000	134137	850	7126	111	6550	598	31279		265	2502.32	10616	117	7160	97
Black Powder	P15_13Aug07_07	6000	130063	811	5988	89	7764	640	33574		251	2685.92	5900	88	4368	86
Black Powder	P15_15Aug07_19	6000	126446	890	6620	98	8280	918	34722		3000	2777.76	7402	96	4461	80
C-4	P15_07Aug07_17	3997	92481	713					11409		200	912.72	9208	109	7648	102
C-4	P15_08Aug07_13	5998	134464	861					16459		184	1316.72	5922	90	5198	81
C-4	P15_10Aug07_07	5997	135085	895					14282		203	1142.56	3750	75	2945	67
C-4	P15_14Aug07_07	6000														
C-4	P15_15Aug07_13	5997	122223	874					18234		214	1458.72	5426	89	3810	74
C-4	P15_16Aug07_07	5998	110248	789					18335		209	1466.8	4407	101	5384	119
Red Dot	P15_07Aug07_07	6000	146422	883					40114		332	3209.12	10575	158	9846	154
Red Dot	P15_09Aug07_07	6000	137159	827					44158		297	3532.64	11642	148	14973	185
Red Dot	P15_10Aug07_19	6000	128588	855					30141		159	2411.28	9212	97	6390	83
Red Dot	P15_13Aug07_13	6000	119903	801					43596		267	3487.68	7669	102	9370	123

TNT	P15_07Aug07_13	6000	135368	798		34089	304	2727.12	13575	128	11007	119	
TNT	P15_08Aug07_19	6000	135127	814		33438	248	2675.04	9824	112	7732	99	
TNT	P15_09Aug07_19	6000	136802	850		33717	251	2697.36	11793	117	8944	104	
TNT	P15_10Aug07_13	6000	120694	806									
TNT	P15_13Aug07_19	6000	118782	796		37096	246	2967.68	10993	117	8000	98	
TNT	P15_15Aug07_07	6000	125042	840		31015	271	2481.2	7596	121	7225	131	
TNT	P15_16Aug07_13	6000	118546	850		30786	237	2462.88	5899	93	4784	90	
Z-powder	P15_29Aug07_07	6000	121558	879		25744	254	2059.52	10267	166	15637	200	
Z-powder	P15_30Aug07_07	6000	118735	873		28027	298	2242.16	13303	195	14743	193	
Z-powder	P15_30Aug07_13	6000	124235	885		26244	269	2099.52	9294	119	11995	181	
Z-powder	P15_05Sep07_13	6000	119256	809		29876	286	2390.08	12756	159	16091	223	
Detasheet	P15_19Jul07_08	6000	127208	718		34861	333	2788.88	12282	155	17556	190	
Detasheet	P15_19Jul07_20	6000	122116	704		31708	336	2536.64	14294	140	13776	134	
Detasheet	P15_24Jul07_08	6000	122969	741		27195	246	2175.6	8174	124	12121	157	
Detasheet	P15_26Jul07_13	6000	112659	736		29074	251	2325.92	10995	122	9317	110	
Semtex 1-A	P15_17Jul07_20	6000	129841	696		31761	321	2540.88	14899	148	13751	135	
Semtex 1-A	P15_18Jul07_08	6000	125055	684		31473	336	2517.84	9314	126	8347	136	
Semtex 1-A	P15_19Jul07_14	6000	120760	685		30203	322	2416.24	12278	130	10179	116	
Semtex 1-A	P15_24Jul07_14	6000	125925	763		26320	236	2105.6	11195	123	7551	99	

Explosive Measurements DT source

Explosive	File-ID	Live Time	Pb-2614	unc	H-2223	unc	S-2230	unc	C-4439	unc	O-5618	unc	O-6129	unc	N-10318	10829
Black Powder	P30_18Jan08_03	3000	79285	449	19068	1320	22151	1122	33479	2678.32	14396	183	17547	184	-11.525	-15.4375
Black Powder	P30_18Jan08_08	2000	48116	350	13832	1000	8519	1000	27727	2218.16	10883	156	11474	148	-1.125	30.8875
Black Powder	P30_18Jan08_11	2000	51241	359	8912	987	12334	859	21294	1703.52	10920	149	11179	145	17.7875	-1.3625
Black Powder	P30_19Jan08_03	3000	107655	574	12884	889	16780	785	33408	2672.64	12613	166	14841	161	-47.65	36.2875
Black Powder	P30_19Jan08_06	3000	65569	448	14170	1801	14062	1303	29069	2325.52	11791	146	14303	150	27.5625	-7.825
Black Powder	P30_19Jan08_10	4000	90887	495	17080	2401	16912	1946	32793	2623.44	16045	165	19187	182	47.025	44.0125
Black Powder	P30_19Jan08_14	4000	86536	494	17278	2757	16378	2046	37337	2986.96	16799	185	20187	182	23.725	31.1125
C-4	P30_08Dec07_03	3000	76015	407	26524	205			23874	1909.92	7958	122	7907	119	171.25	56.737
C-4	P30_08Dec07_06	3000	75586	458	37654	232			23282	1862.56	8836	124	9755	127	200.24	136.61
C-4	P30_08Dec07_09	3000	72683	424	37203	227			25508	2040.64	8374	128	8189	124	167.68	115.13
C-4	P30_08Dec07_12	2500	60859	426	50202	262			21826	1746.08	8086	137	9093	132	195.7	177.3
C-4	P30_15Dec07_14	3000	81635	432	42844	251			24947	1995.76	10321	140	10176	129	23.3125	13.175
Detasheet	P30_25Jan08_03	3000	69967	444	24024	207			21457	1716.56	7513	120	8513	132	81.15	23.3875

Detasheet	P30_25Jan08_06	3000	70619	432	21543	205	21431	1714.48	9739	140	9314	138	38.09999	46.025
Detasheet	P30_25Jan08_09	2500	60524	417	17638	185	19712	1576.96	7542	136	7962	130	-15.1	-14.275
Detasheet	P30_26Jan08_03	3000	75195	462	27267	225	30872	2469.76	10318	166	9183	159	19.7875	-37.9625
Detasheet	P30_26Jan08_06	3000	70802	453	27015	232	30677	2454.16	11332	169	12276	189	-3.9375	-3.35
Detagel	P10_11Apr08_12	3000	54471	459	129562	475	31127	522	32495	273	27834	270	354.625	145.525
Detagel	P10_11Apr08_09	3000	53504	407	126174	457	20514	474	30815	263	26395	273	286.95	212.087
Detagel	P10_11Apr08_06	3000	51886	555	125110	459	25223	501	30128	256	25860	261	288.25	169.58
Detagel	P10_11Apr08_03	3000	51286	595	128688	467	23857	475	33514	298	27655	295	341.625	177.575
Red Dot	P30_14Dec07_03	3000	79468	458	10746	148	26045	2083.6	8325	125	12073	141	18.6625	10.7625
Red Dot	P30_14Dec07_05	2000	50758	360	12409	160	19745	1579.6	7822	118	8605	121	24.7999	9
Red Dot	P30_14Dec07_08	3000	75148	408	12400	234	30031	2402.48	10685	141	11375	139	72.7625	6.95
Red Dot	P30_14Dec07_11	3000	75745	401	12672	167	31433	2514.64	11130	139	10763	138	2.325	16.525
Red Dot	P30_15Dec07_06	3000	92576	467	14464	216	31218	2497.44	12450	168	12359	167	5.1	67.5875
Red Dot	P30_15Dec07_11	5000	127756	543	36783	265	52699	4215.92	18932	206	19853	187	76.6999	90.849
Semtex 1-A	P30_22Feb08_06	6000	167151	690	14946	136	23756	1900.48	6561	107	7602	110	-9.0625	-43.375
Semtex 1-A	P30_22Feb08_12	6000	168509	687	14670	125	25865	2069.2	7224	96	7179	99	6.1375	37.9875
Semtex 1-A	P30_22Feb08_14	2000	55951	382	4291	70	7096	567.68	2415	49	2414	49	44.3625	-4.575
Semtex 1-A	P30_23Feb08_06	6000	153117	624	11644	144	20013	1601.04	5379	145	6193	123	-57.2	46.3125
Semtex 1-A	P30_23Feb08_09	3000	71917	433	6227	96	9554	764.32	2964	70	3812	75	-3.4625	-21.5375
TNT	P30_26Jan08_10	4000	98115	521	25267	250	54732	4378.56	13369	175	10568	162	75.0376	-34.775
TNT	P30_09Feb08_04	4000	108753	570	31851	265	67698	5415.84	17258	203	16852	205	46.4	-13.175
TNT	P30_09Feb08_09	4000	115176	583	28492	209	73560	5884.8	16072	179	16792	207	34.9875	35.7001
Z-Powder	P15_30May08_03	3000	51423	480	39289	314	39782	495	31854	239	35063	256	248.423	162.4286
Z-Powder	P15_30May08_06	3000	45974	800	42521	355	31735	454	27461	232	30356	234	245.1968	166.9187
Z-Powder	P15_30May08_09	3000	46590	542	43720	381	35381	499	28389	229	31428	221	245.9872	170.7929
Z-Powder	P15_30May08_12	3000	45289	782	41801	352	38281	501	32053	237	35552	241	251.424	179.4

Black Powder Explosive, Sulfur and Potassium Peaks DT source

Explosive	File-ID	Live Time	Pb-2614	unc	H-2223	unc	S-2230	K-2813	unc	unc	C-4439	unc	O-5618	unc	O-6129	unc

Black Powder	P30_18Jan08_03	3000	79285	449	19068	1320	22151	9853	353	1122	33479	2678.32	14396	183	17547	184
Black Powder	P30_18Jan08_08	2000	48116	350	13832	1000	8519	7224	321	1000	27727	2218.16	10883	156	11474	148
Black Powder	P30_18Jan08_11	2000	51241	359	8912	987	12334	6117	257	859	21294	1703.52	10920	149	11179	145
Black Powder	P30_19Jan08_03	3000	107655	574	12884	889	16780	8488	304	785	33408	2672.64	12613	166	14841	161
Black Powder	P30_19Jan08_06	3000	65569	448	14170	1801	14062	9065	298	1303	29069	2325.52	11791	146	14303	150
Black Powder	P30_19Jan08_10	4000	90887	495	17080	2401	16912	11541	337	1946	32793	2623.44	16045	165	19187	182
Black Powder	P30_19Jan08_14	4000	86536	494	17278	2757	16378	11592	342	2046	37337	2986.96	16799	185	20187	182

Appendix B

Spectral Overlays for Explosives and Simulants

Appendix B

Spectral Overlays for Explosives and Simulants

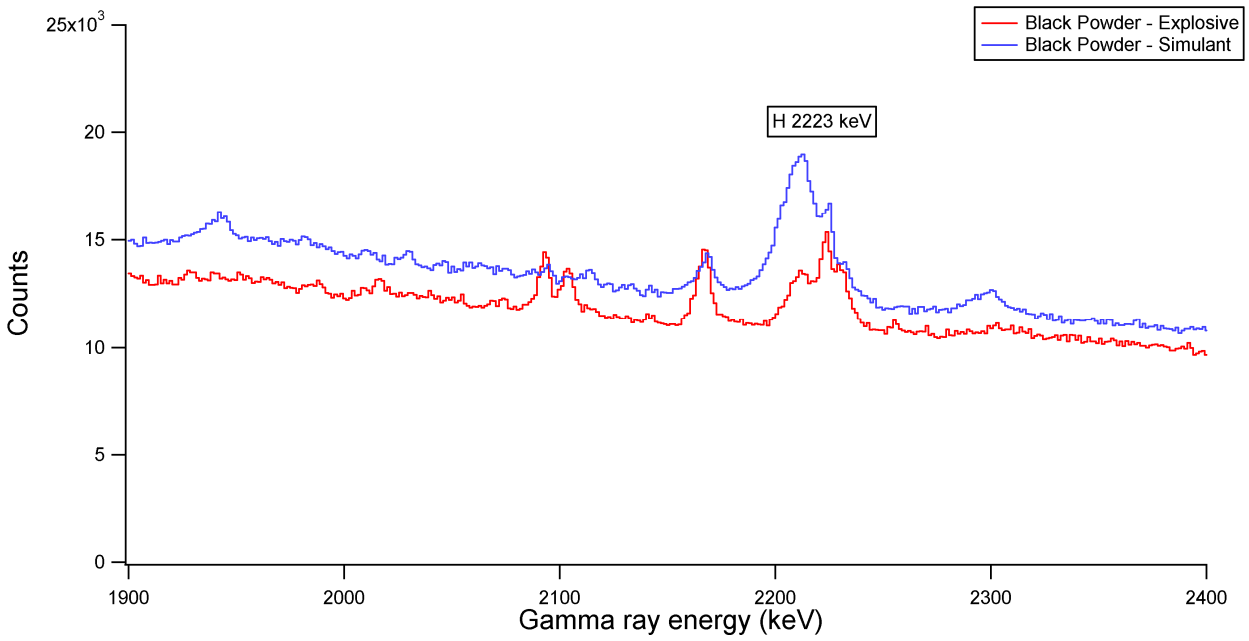

Figure B1. Hydrogen region of black powder explosive and simulant spectrat

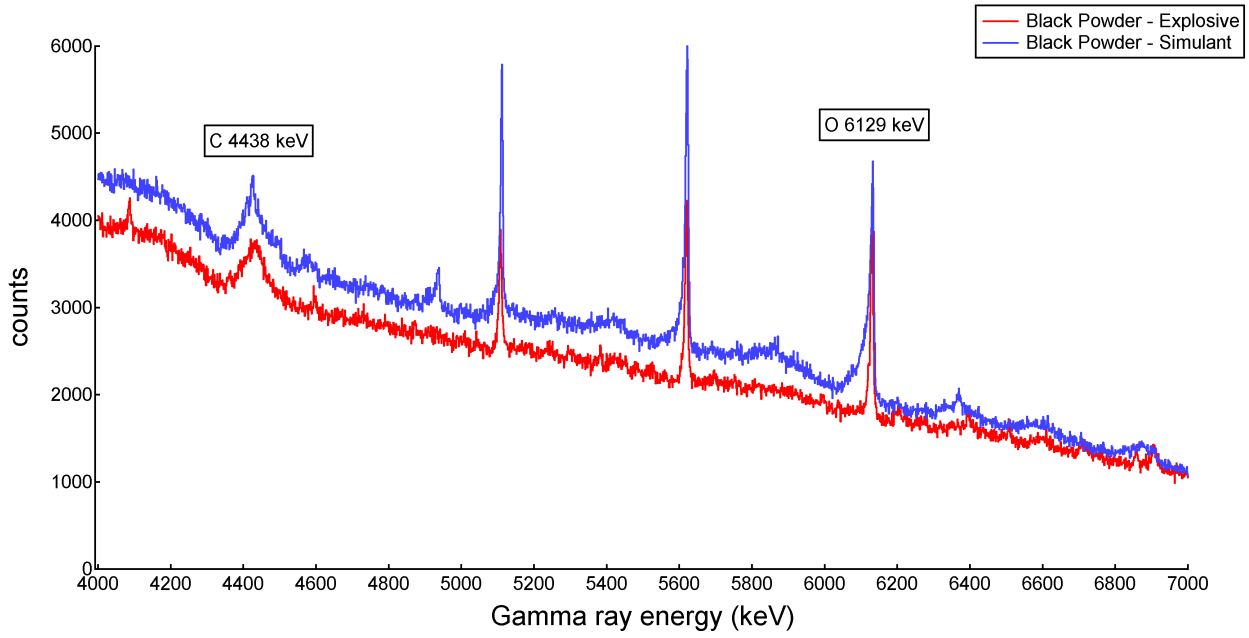

Figure B2. Oxygen region of black powder explosive and simulant spectra

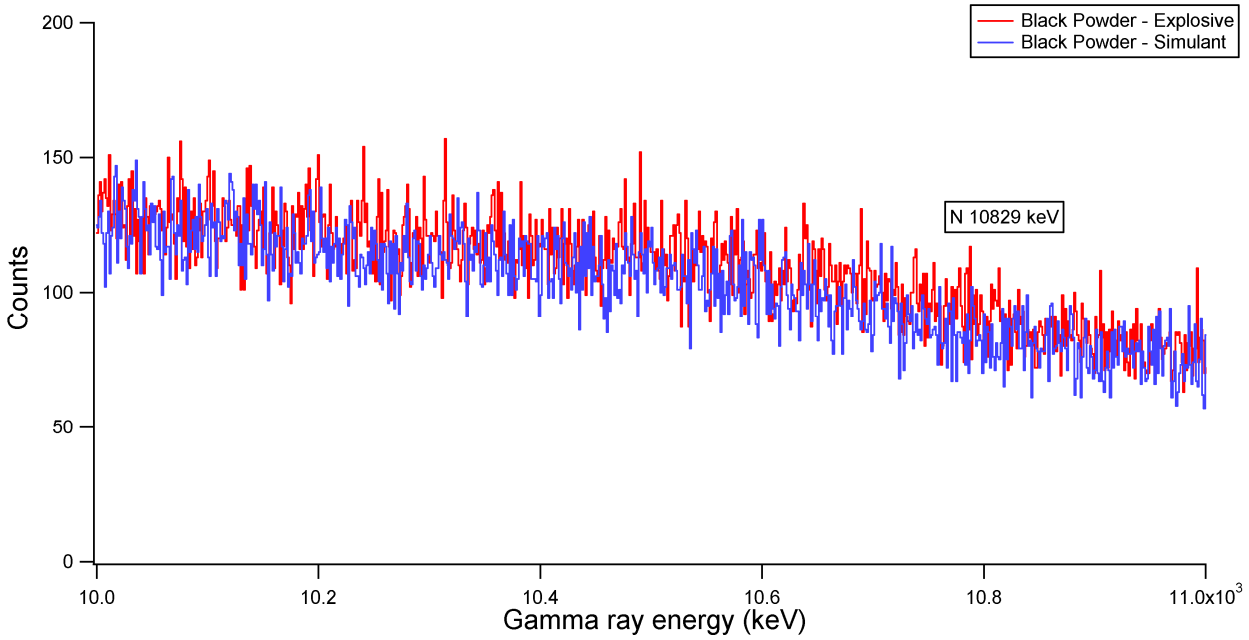

Figure B3. Nitrogen region of black powder explosive and simulant spectra.

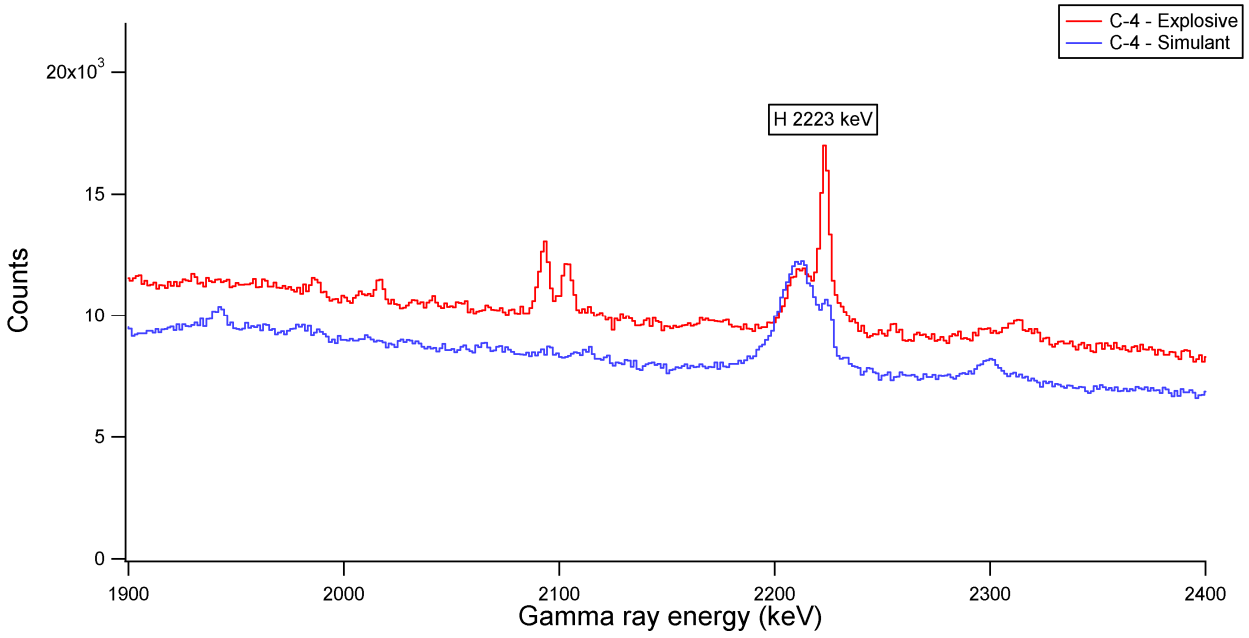

Figure B4. Hydrogen region of C-4 explosive and simulant spectra.

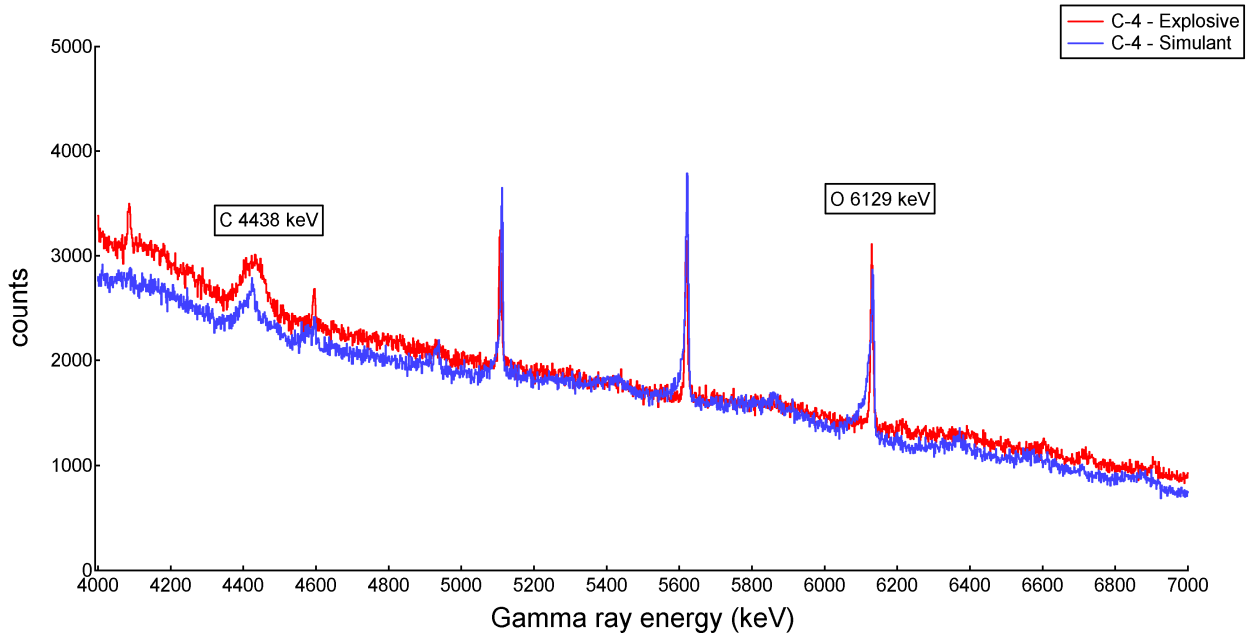

Figure B5. Oxygen region of C-4 explosive and simulant spectra

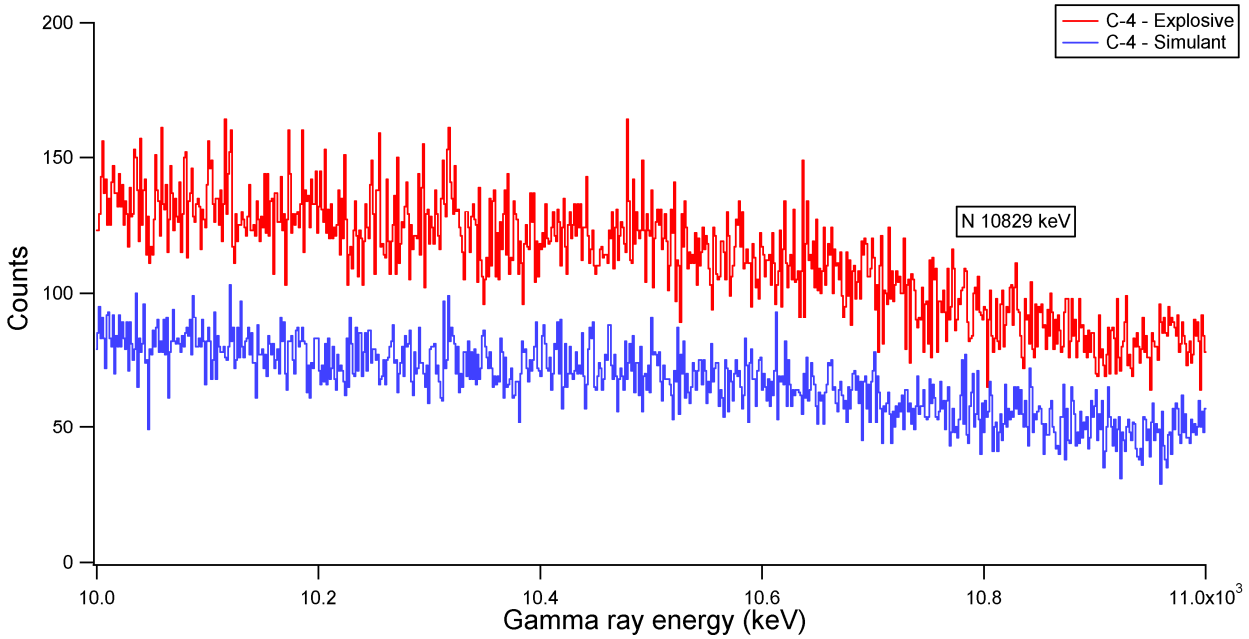

Figure B6. Nitrogen region of C-4 explosive and simulant spectra.

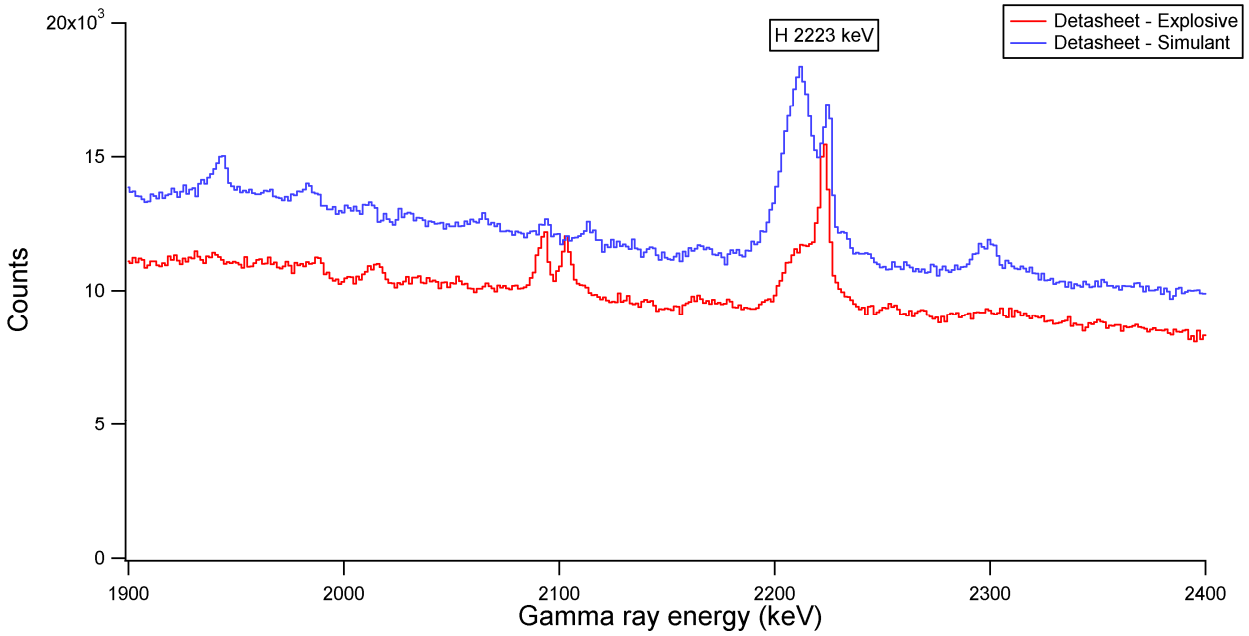

Figure B7. Hydrogen region of Detasheet explosive and simulant spectra.

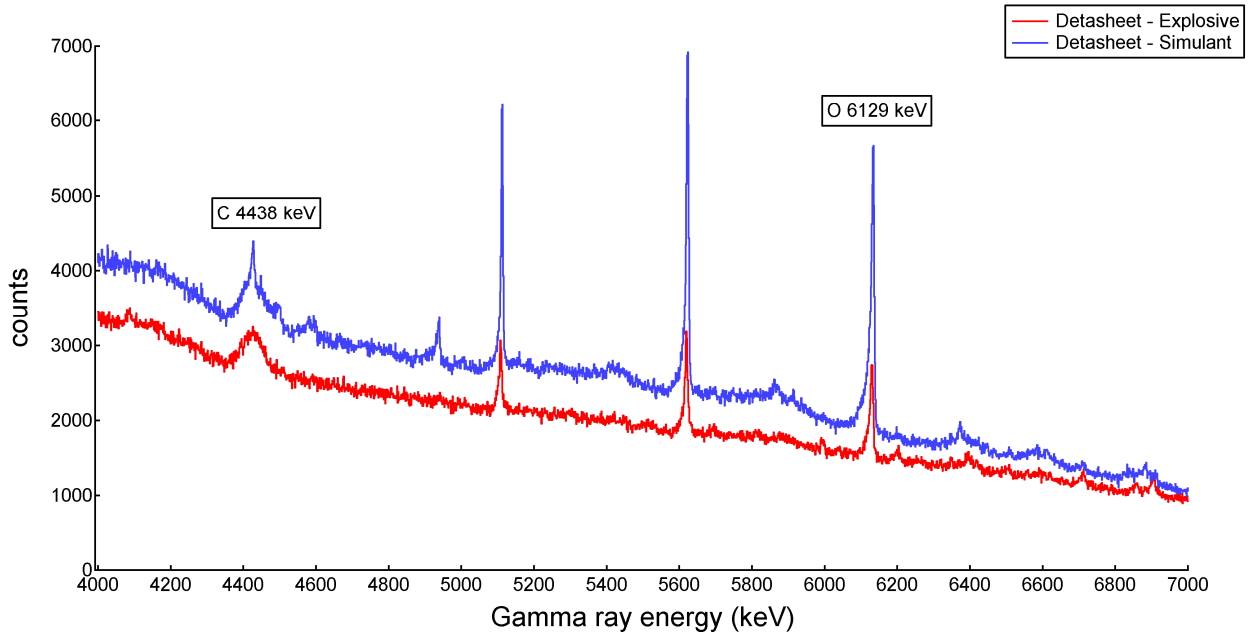

Figure B8. Oxygen region of Detasheet explosive and simulant spectra.

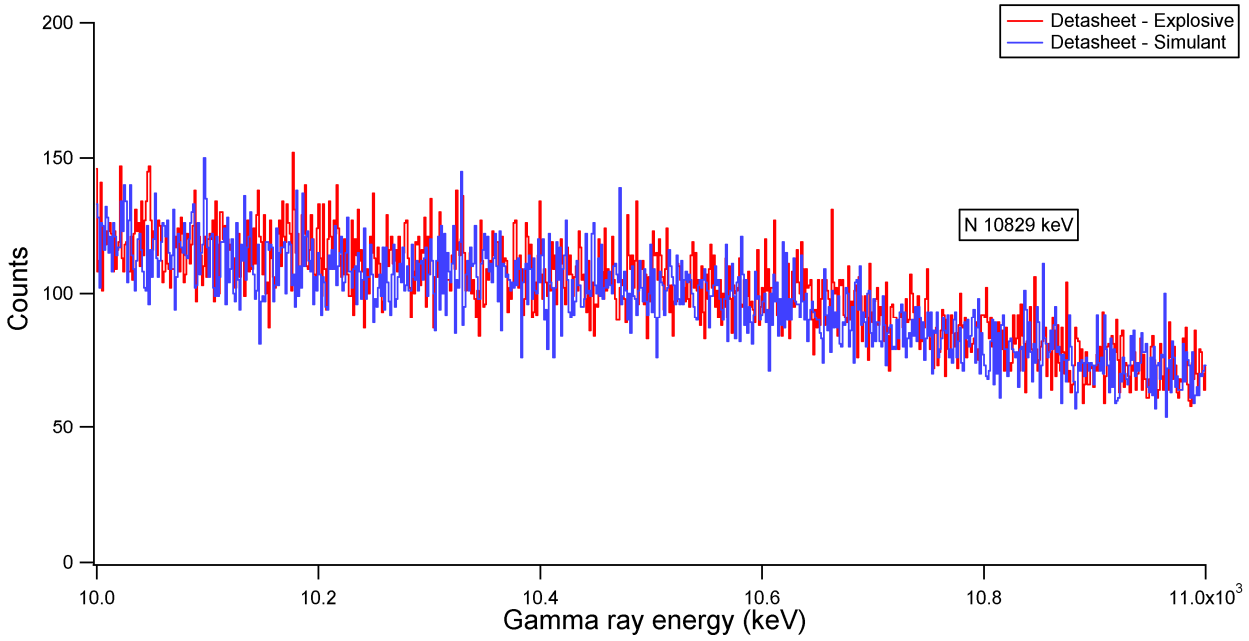

Figure B9. Nitrogen region of Detasheet explosive and simulant spectra.

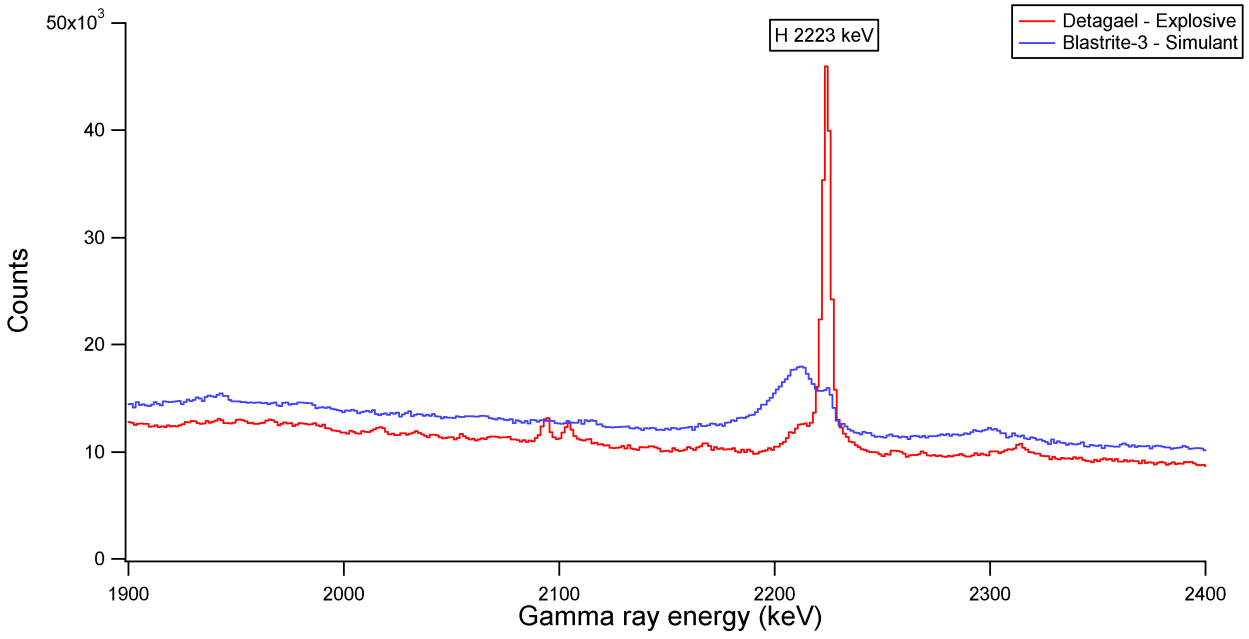

Figure B10. Hydrogen region of Detagel explosive and Blastrite-3 simulant spectra.

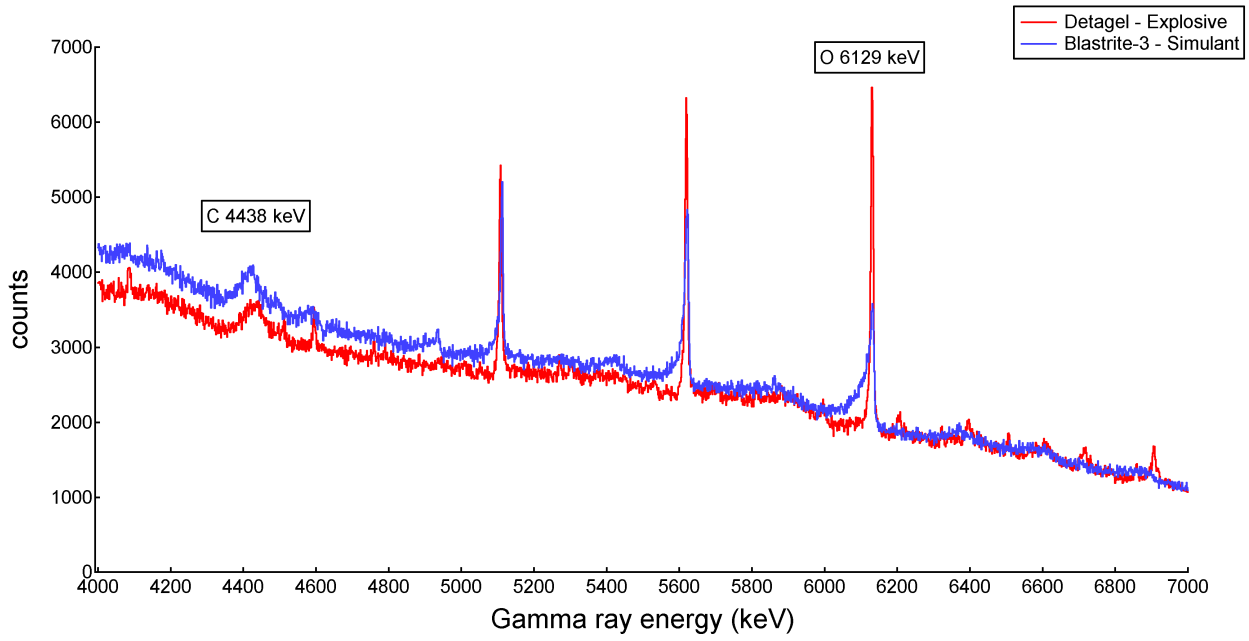

Figure B11. Oxygen region of Detagel explosive and Blastrite-3 simulant spectra.

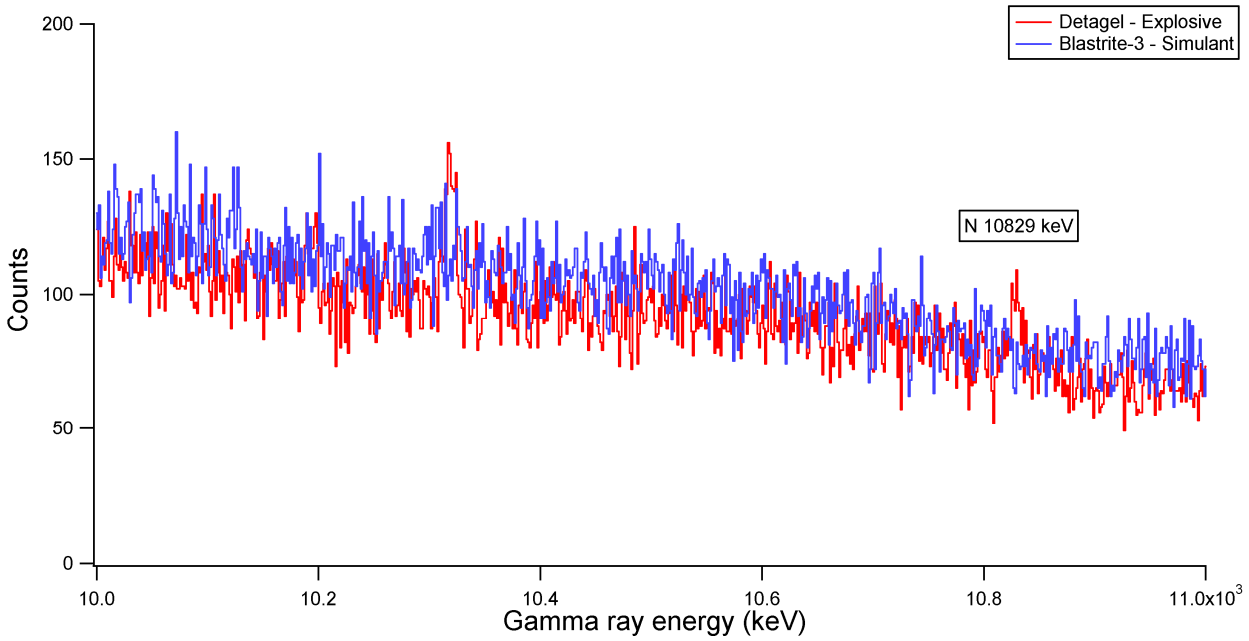

Figure B12. Nitrogen region of Detagel explosive and Blastrite-3 simulant spectra.

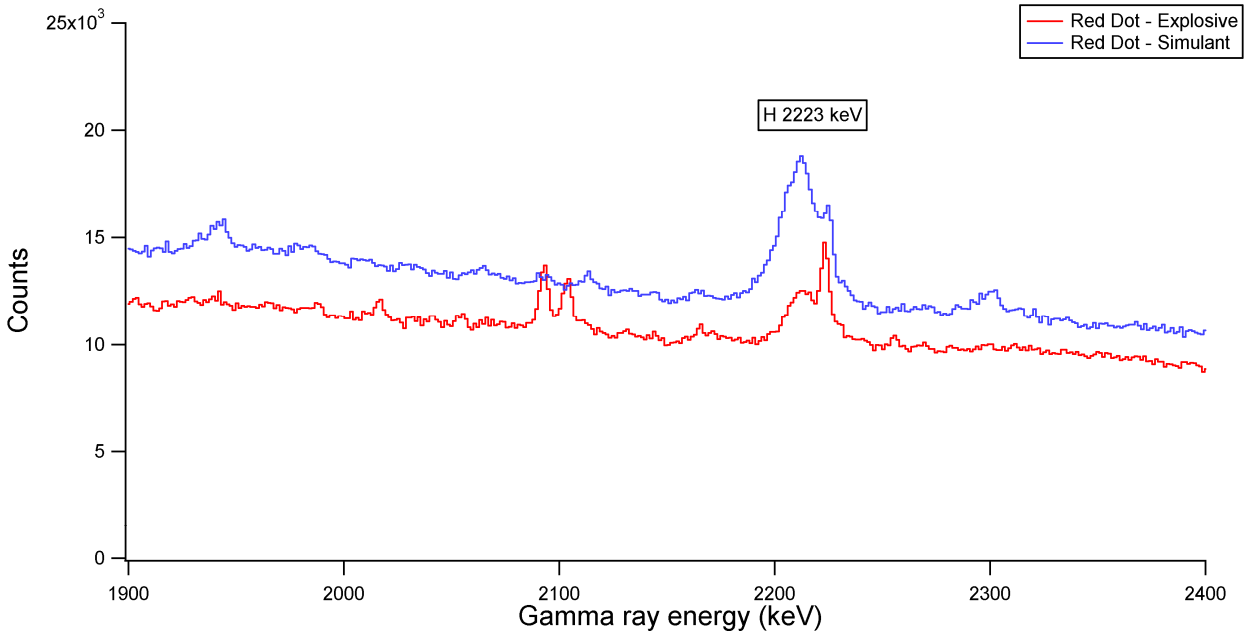

Figure B13. Hydrogen region of Red Dot explosive and simulant spectra.

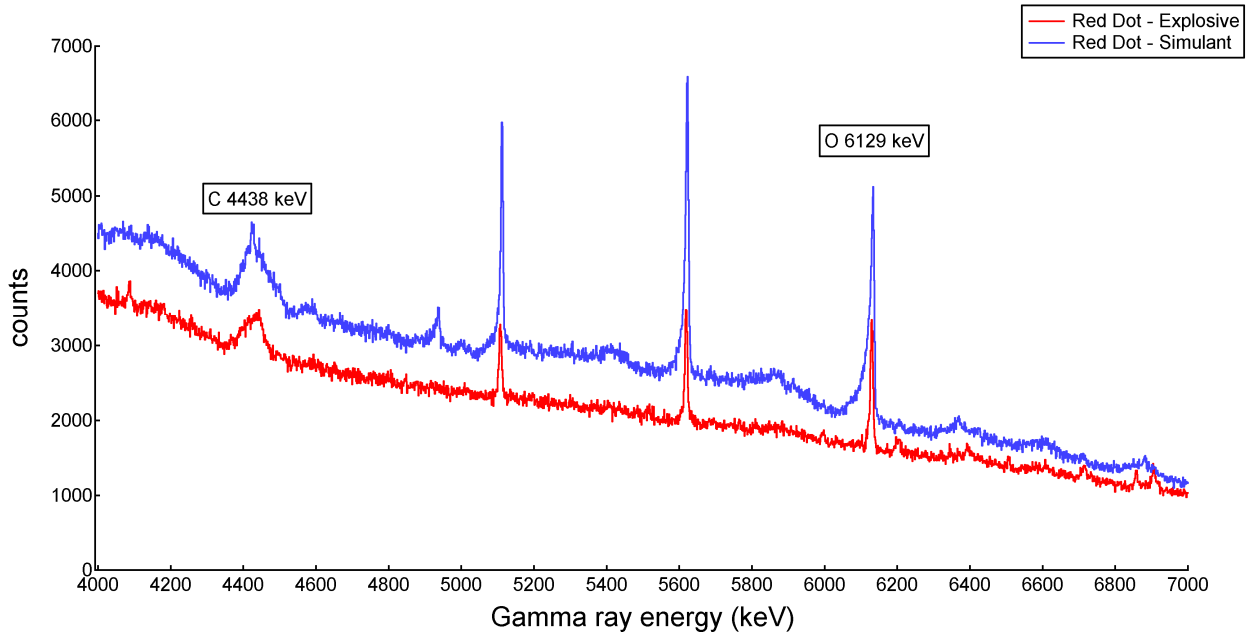

Figure B14. Oxygen region of Red Dot explosive and simulant spectra.

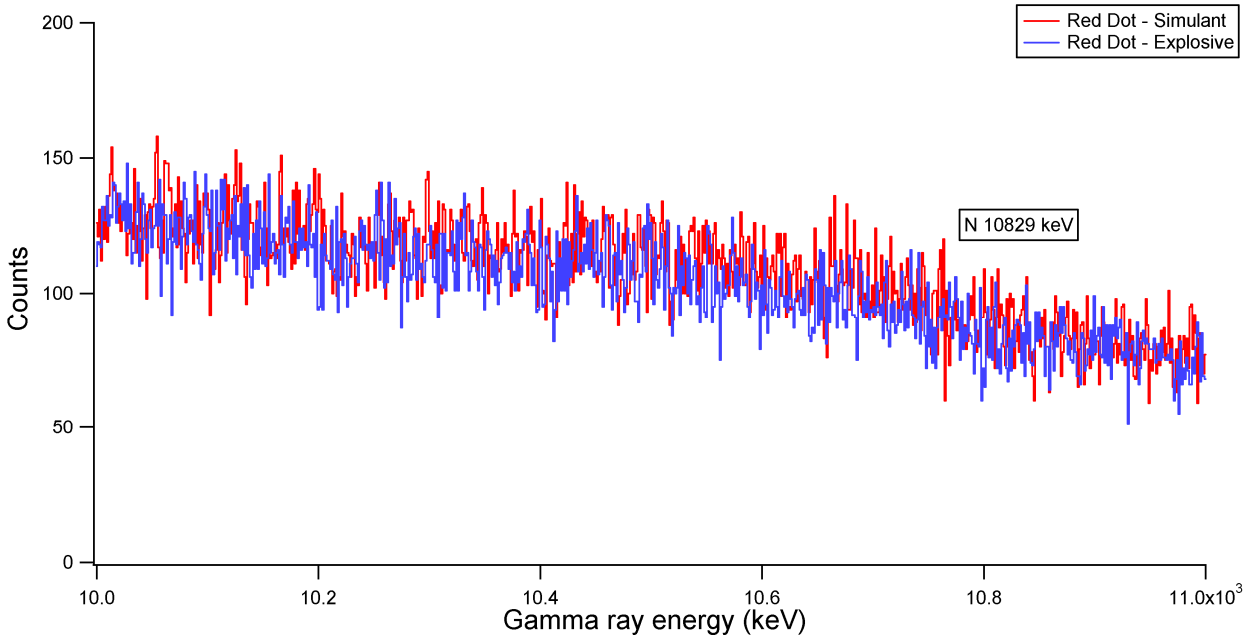

Figure B15. Nitrogen region of Red Dot explosive and simulant spectra.

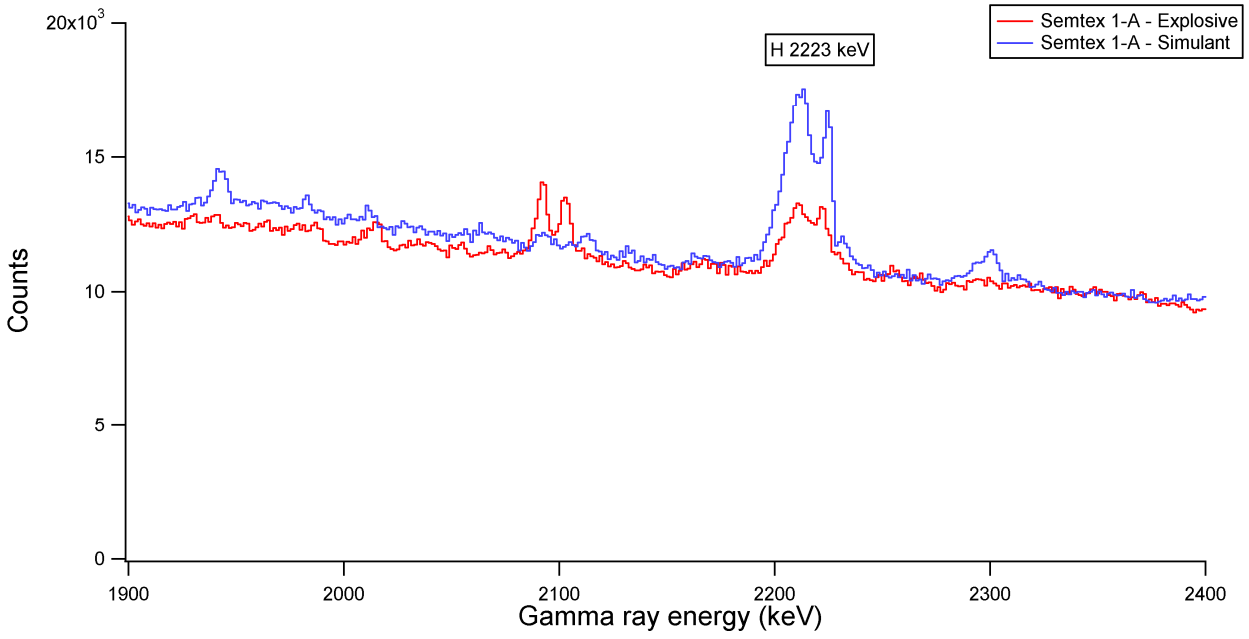

Figure B16. Hydrogen region of Semtex 1-A explosive and simulant spectra.

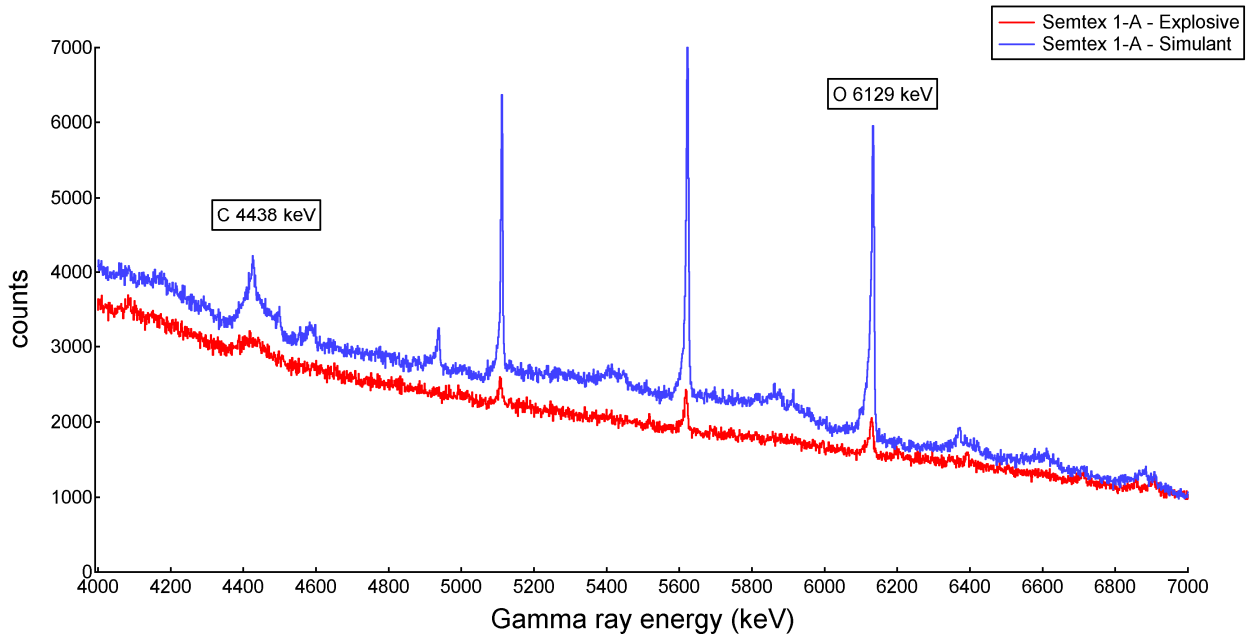

Figure B17. Oxygen region of Semtex 1-A explosive and simulant spectra.

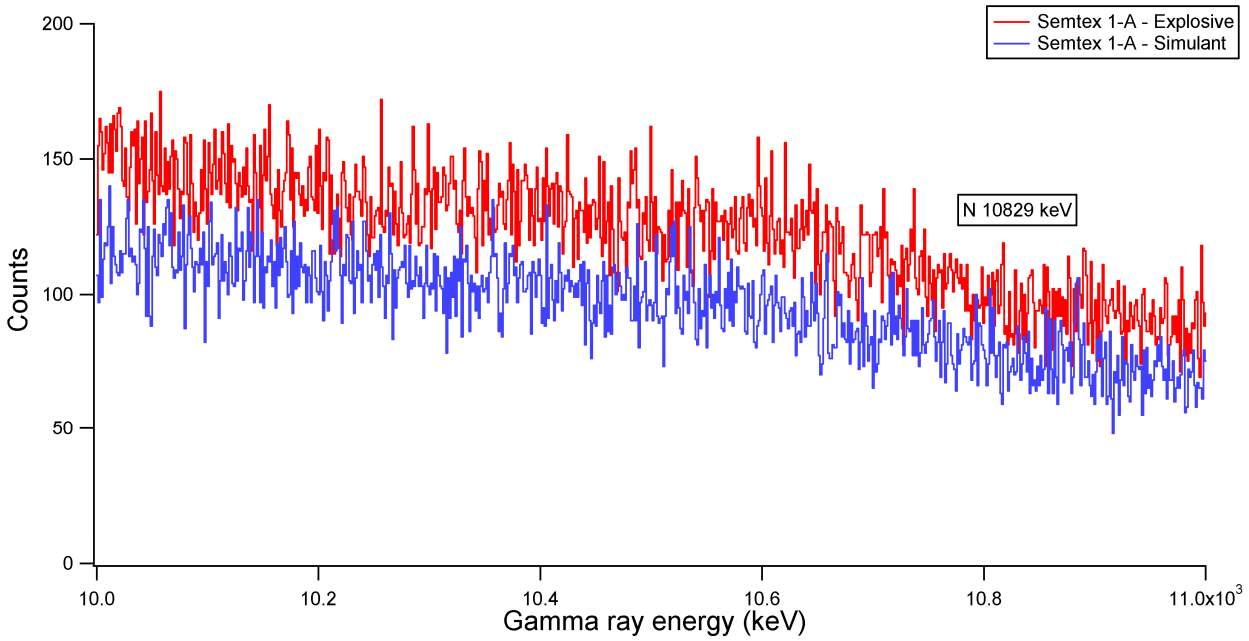

Figure B18. Nitrogen region of Semtex 1-A explosive and simulant spectra.

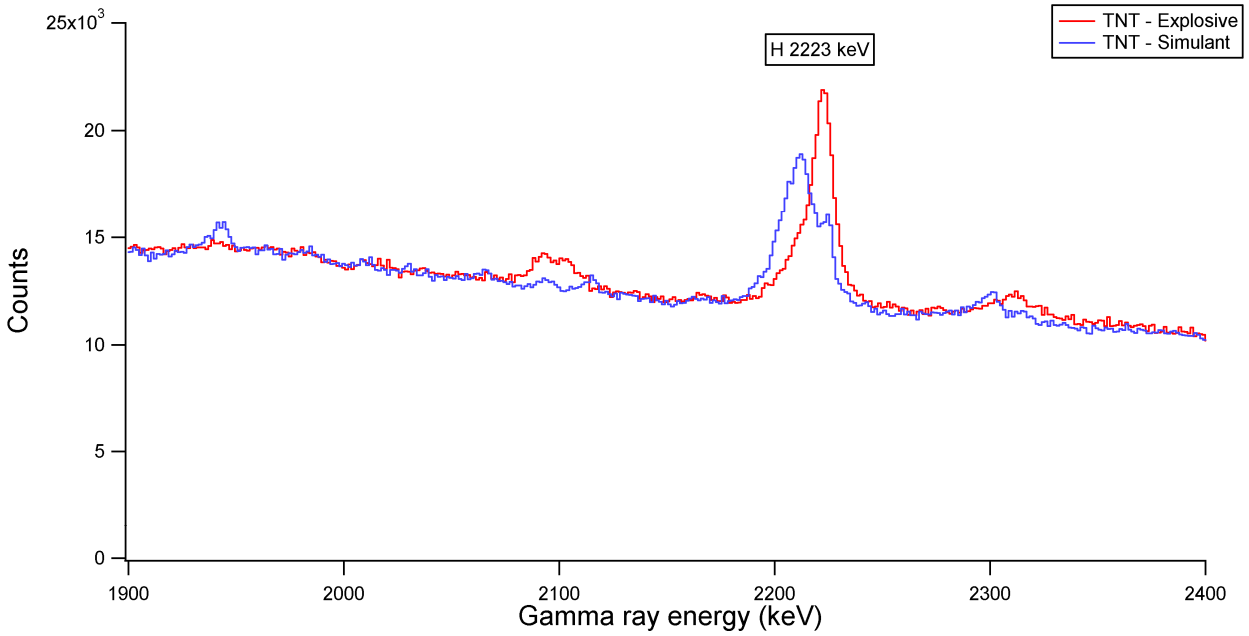

Figure B19. Hydrogen region of TNT explosive and simulant spectra.

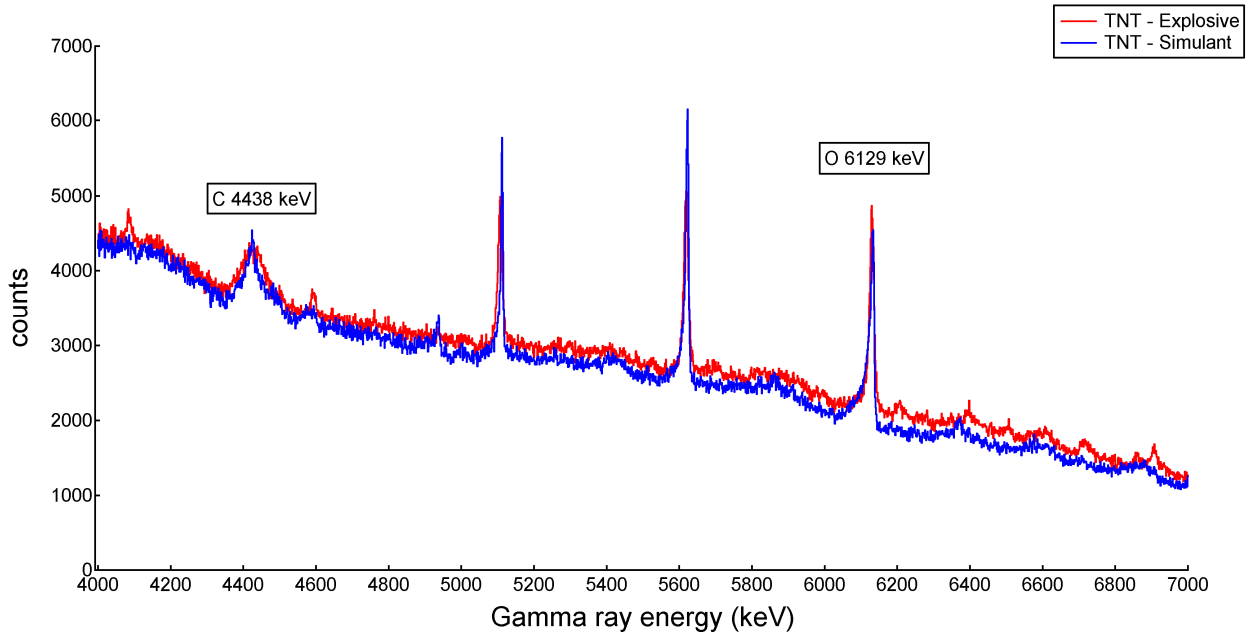

Figure B20. Oxygen region of TNT explosive and simulant spectra.

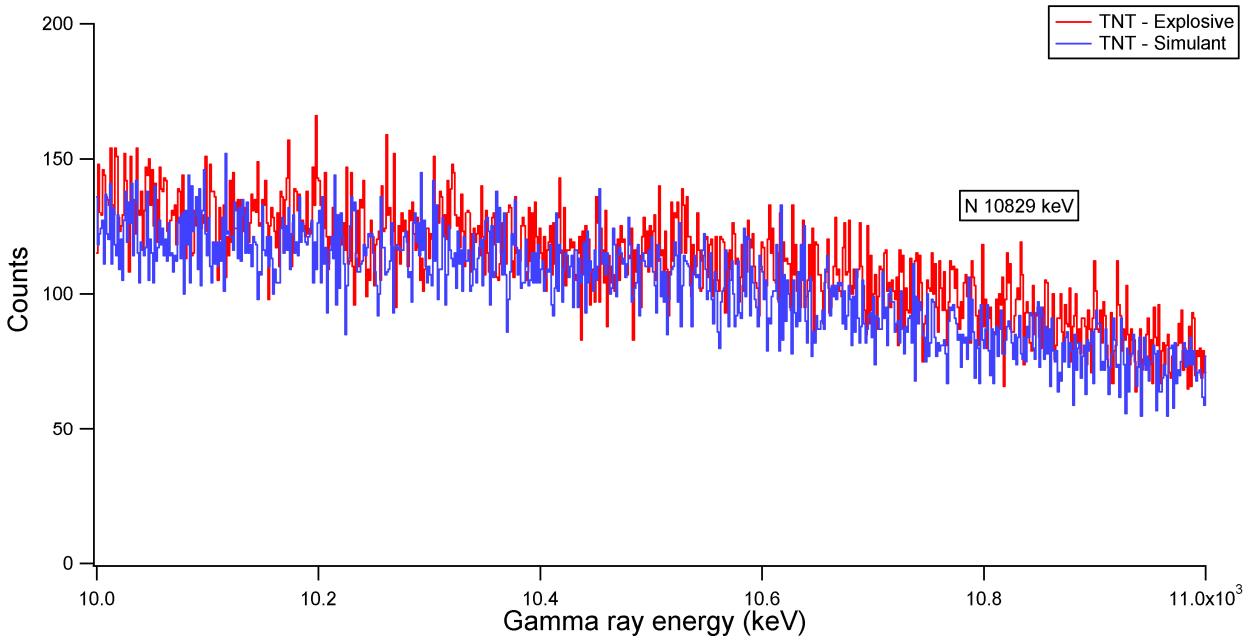

Figure B21. Nitrogen region of TNT explosive and simulant spectra.

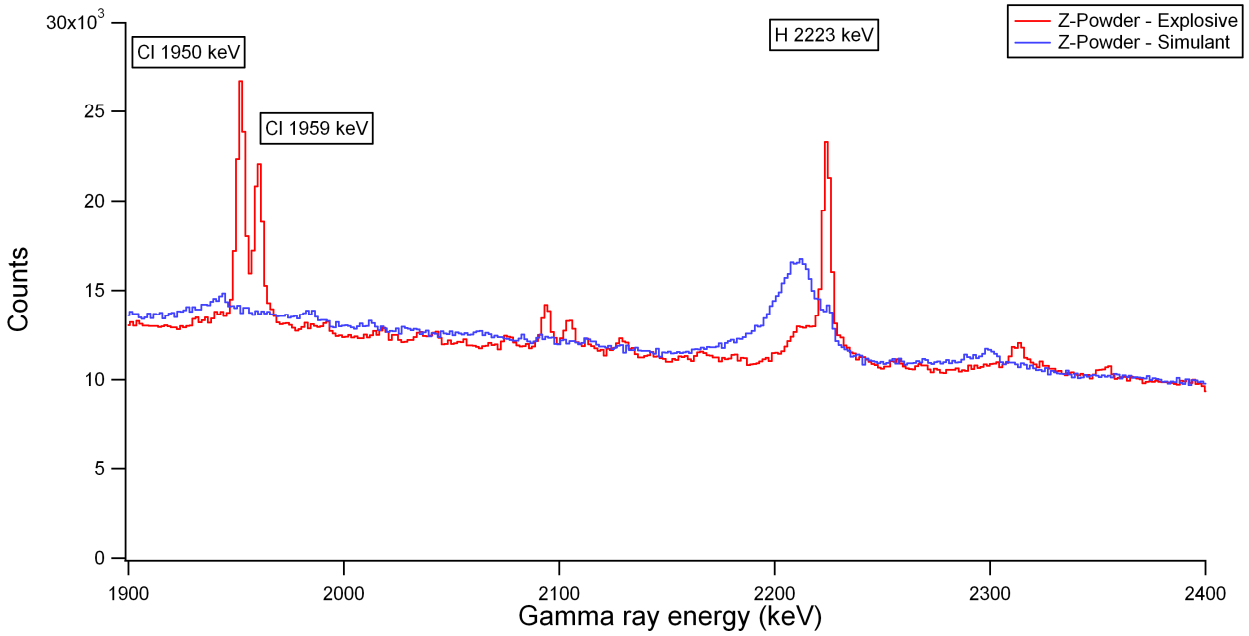

Figure B22. Hydrogen region of Z-Powder explosive and simulant spectra.

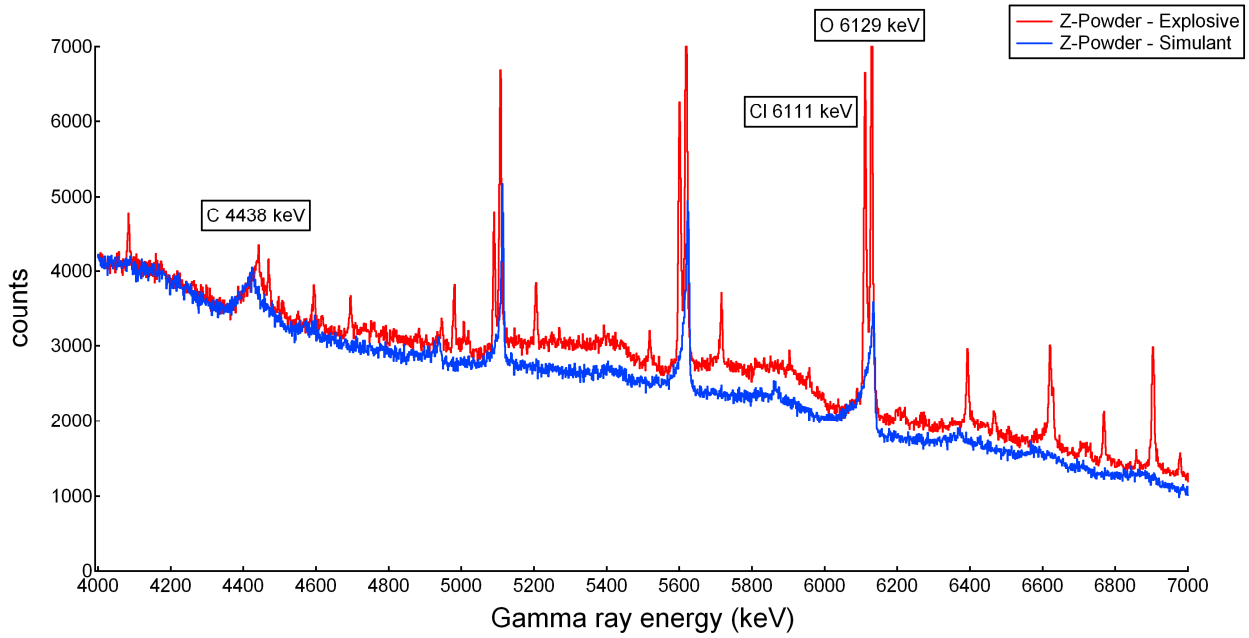

Figure B23. Carbon region of Z-Powder explosive and simulant spectra.

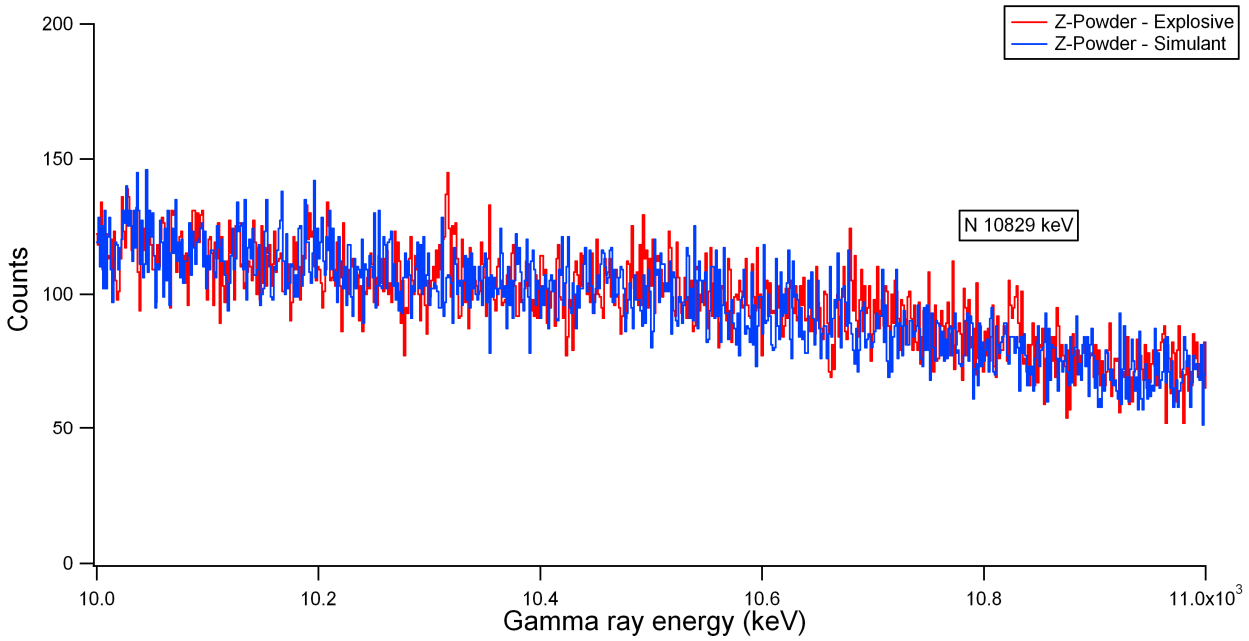

Figure B24. Nitrogen region of Z-Powder explosive and simulant spectra.